Characterization of Unique Eukaryotic Sphingolipids with Temperature-Dependent Δ8-Unsaturation from the Picoalga Ostreococcus tauri

Toshiki Ishikawa, Frédéric Domergue, Alberto Amato, Florence Corellou

▶ **To cite this version:**

Toshiki Ishikawa, Frédéric Domergue, Alberto Amato, Florence Corellou. Characterization of Unique Eukaryotic Sphingolipids with Temperature-Dependent Δ8-Unsaturation from the Picoalga Ostreococcus tauri. Plant and Cell Physiology, 2024, 65 (6), pp.1029-1046. ⟨10.1093/pcp/pcae007⟩. ⟨hal-04746978⟩

HAL Id: hal-04746978

https://hal.science/hal-04746978v1

Submitted on 21 Oct 2024

HAL is a multi-disciplinary open access archive for the deposit and dissemination of scientific research documents, whether they are published or not. The documents may come from teaching and research institutions in France or abroad, or from public or private research centers.

L'archive ouverte pluridisciplinaire **HAL**, est destinée au dépôt et à la diffusion de documents scientifiques de niveau recherche, publiés ou non, émanant des établissements d'enseignement et de recherche français ou étrangers, des laboratoires publics ou privés.

HAL Authorization

CHARACTERISATION OF UNIQUE EUKARYOTIC SPHINGOLIPIDS WITH TEMPERATURE-DEPENDENT Δ8-UNSATURATION FROM THE PICOALGA OSTREOCOCCUS TAURI

One sentence summary: O. tauri sphingolipids are acidic glycosylceramides whose D8-unsaturation varies with temperature.

Short title: *O. tauri* sphingolipids and temperature acclimation

Toshiki Ishikawa[1], Frédéric Domergue[2], Alberto Amato[3], Florence Corellou[3*]

*Corresponding author

Author's affiliation:

1- Graduate School of Science and Engineering, Saitama University, 225 Shimo-Okubo, Sakura-ku, Saitama-city, Saitama, 338-8570, Japan.

2- University of Bordeaux, CNRS, LBM, UMR 5200, Villenave d'Ornon, France

3- Univ. Grenoble Alpes, CNRS, CEA, INRAE, IRIG, LPCV, 38000 Grenoble, France.

SUMMARY

Sphingolipids are ubiquitous components of eukaryotic cell membranes and are found in some prokaryotic organisms and viruses. They are composed of a sphingoid backbone that may be acylated and glycosylated. Assembly of various sphingoid base, fatty-acyl and glycosyl moieties results in highly diverse structures. The functional significance of variations in sphingolipid chemical diversity and abundance is still in the early stages of investigation. Among sphingolipid modifications, the Δ8-desaturation of the sphingoid base occurs only in plant and fungi. In plant, sphingolipid Δ8-unsaturation is involved in cold-hardiness. Our knowledge of the structure and functions of sphingolipids in microalgae lags far behind that of animals, plants and fungi. Original sphingolipid structures have been reported from microalgae. However, functional studies are still missing. *Ostreococcus tauri* is a minimal microalga at the base of the green lineage, and is therefore a key organism for understanding lipid evolution. In the present work, we achieved the detailed characterisation of *O. tauri* sphingolipids and unveiled unique glycosylceramides as sole complex sphingolipids. The head groups are reminiscent of bacterial sphingolipids, as they contain hexuronic acid residues and can be polyglycosylated. Ceramide backbones show limited variety and sphingolipid

modification is restricted to Δ8-unsaturation. The Δ8-sphingolipid desaturase from *O. tauri* only produced *E*-isomers. Expression of Δ8-sphingolipid desaturase and Δ8-unsaturation of spingolipids both varied with temperature, with lower levels at 24°C than at 14°C. Overexpression of the Δ8-sphingolipid desaturase dramatically increases the level of Δ8 unsaturation at 24°C and is paralleled by a failure to increase cell-size. Our work provides the first characterisation of *O. tauri* sphingolipids and functional evidence for the involvement of sphingolipid Δ8-unsaturation for temperature acclimation in microalgae, suggesting that this function is an ancestral feature in the green lineage.

INTRODUCTION

Sphingolipids (SLs) are fundamental components of cellular membranes and bioactive signalling molecules (Hannich et al., 2011). Microalgae are taxonomically diverse and comprise the earliest divergences within the major multicellular lineages such as plants and seaweeds (Hopes and Mock, 2015). Gaining insight into the molecular nature and regulation of SLs in microalgae is therefore fundamental to shed light on the structure/function of these compounds.

The ceramide (Cer) backbone of SLs is constituted of a long chain base (LCB) linked to a fatty acyl chain (FA) via an amide bond (Mashima et al., 2019). LCBs and FAs vary in carbon chain length, degree of unsaturation, number and/or position of hydroxyl groups. Complex SLs further display a polar head group consisting of variable glycosyl residues attached to the non-polar ceramide. Glycosylsphingolipids (GSLs) can be divided into glycosylceramides (GlyCers) and into glycosylinositolphosphorylceramides (GIPCs) (Haslam and Feussner, 2022). GlyCers have a sugar polar head directly linked to the Cer moiety whereas the core structure of polar head in GIPCs consist of an inositol-glucuronic-acid linked to the Cer via a phosphodiester bond. Polar heads of GlyCers commonly contain only one sugar residue while that of GIPCs are polyglycosylated. Polyglycosylated GlyCers however occur in some non-green microalgae as well as in proteobateria from the *Sphingomonad* genus (Kawahara et al., 1991; Kawahara et al., 2000). Plant GIPCs contain up to seven different sugar moieties. In plants, GIPCs are the dominant SLs constituting 64 % of the total in *Arabidopsis thaliana* leaves against 34 % for GlyCers (Markham and Jaworski, 2007). Whether SLs are channelled into GlyCer or GIPC formation is likely determined by LCB modifications (Chen et al., 2012).

LCBs modifications include desaturations, hydroxylation, and, in fungi, methylation. LCB-Δ4-desaturation is widespread in eukaryotes while Δ8-desaturation only occurs in plants and fungi in conjunction with either 4-desaturation or 4-hydroxylation (Mashima et al., 2019; Huby et al., 2020; Haslam and Feussner, 2022). Since Δ8-unsaturation was detected as the primary monounsaturation of di-hydroxy-LCBs in gymnosperms but only in a few angiosperm species, including *A. thaliana* it was proposed that Δ4-monounsaturation is ancestral (Islam et al., 2012). In *A. thaliana* Δ8-unsaturated LCBs largely dominate in all SLs while Δ4-desaturation mostly occurs in combination with LCB Δ8-desaturation and is restricted to Glucose-Cers (GlcCers) of floral tissues (Michaelson et al., 2009).

Plant LCBs are predominantly C18 amino alcohols and are largely comprised of 4-hydroxysphinganine (t18:0, phytosphingosine) and its desaturated form 4-hydroxy-8-sphingenine (t18:1^{8}) (Michaelson et al., 2016). Other SLs include sphinganine (d18:0 dihydrosphingosine) and its desaturated forms 8-sphingenine (d18:1^{8}), 4-sphingenine (d18:1^{4E} sphingosine) and 4,8-sphingadienine (d18:$2^{4E,8}$). The double bond at the Δ8 position is present in either the cis (*Z*) or the trans (*E*) configurations and the ratios of these isomers vary according to the species. Although, the overall *E*/*Z* ratio does not correlate with chilling sensitivity of plant species, it was proposed that the amount of t18:1^{8Z} correlates with chilling hardiness (Imai et al., 1997).

Sphingolipid Δ8-desaturases (SLD8) are cytochrome b5-fused desaturases that have first been characterised from plants and thereafter identified in fungi (Sperling et al., 1998; Takakuwa et al., 2002). Disruption of SLD8 in *Candida albicans* resulted in reduced hyphal growth at low temperature (Oura and Kajiwara, 2008). Similarly, *A. thaliana* double *sld1 sld2* mutants lacked apparent growth phenotypes under optimal conditions, but displayed advanced chlorosis after prolonged exposure to low temperature (Chen et al., 2012). However, sphingolipid Δ8-unsaturation remained surprisingly unaltered by temperature in wild-type (WT) plants (Nagano et al., 2014). Nevertheless, silencing SLD8 in tomato plants also correlated well with impaired cold-acclimation (Zhou et al., 2016). Although this study did not report how the level of sphingolipid Δ8-unsaturation changed as a function of temperature in wild-type plants, it further supported that SLD8 is functionally involved in plant cold response.

Despite the key phylogenetic position and ecological importance of microalgae, investigations about microalgal SLs structure remain scarce and functional studies are lacking (reviewed in (Stonik and Stonik, 2018)). The green marine picoalga *Ostreococcus tauri*

(Mamiellophyceae, Chlorophyta) corresponds to the most minimalist photosynthetic eukaryote (≈ 1 µm) (Courties et al., 1994; Marin and Melkonian, 2010). *O. tauri* has a strikingly simple cellular organization, with no cell wall or flagella, and with a single chloroplast and mitochondrion, and it further has an extremely reduced genome (≈ 13 Mb) (Derelle et al., 2006; Henderson et al., 2007). *O. tauri* is therefore an ideal model to gain insight into core metabolic and physiological processes. Moreover, *O. tauri* occupies a basal position in the green lineage, which makes this unicellular organism key for elucidating early stages in the history of lipid evolution (Leliaert et al., 2012). We have previously achieved detailed analyses of *O. tauri* glycerolipidome and characterised original FA-desaturases (Degraeve-Guilbault et al., 2017; Degraeve-Guilbault et al., 2020; Degraeve-Guilbault et al., 2021). Interestingly, *O. tauri* lipidic features combine traits found in the green lineage (Archaplastida) and the distantly related eukaryotic supergroup composed of Stramenopiles, Alveolates, Rhizaria (SAR supergroup) (Degraeve-Guilbault et al., 2017; Degraeve-Guilbault et al., 2021). Since SAR have evolved from secondary endosymbiosis, it is reasonable to assume that *O. tauri* might have conserved some ancestral feature that were lost during the evolution of land plants.

In the present work, we sought to better understand the structure and function of *O. tauri* SLs. Through a detailed characterisation of *O. tauri* SLs, we discovered unique classes of GSLs composed of novel sugar head groups and homogeneous ceramides whose only modification is the LCB Δ8-unsaturation. Temperature variations and SLD8 overexpression were then used to shed light on the physiological role of LCB desaturation in *O. tauri*.

RESULTS

Characterisation of *O. tauri* sphingolipids

First, we analysed the structure of *O. tauri* SLs. Dried cells were directly subjected to strong alkaline hydrolysis for comprehensive profiling of LCB species liberated from SLs (Markham et al., 2006). LC-MS/MS analysis of total LCBs revealed that *O. tauri* displays only two major LCBs: sphinganine (d18:0) and its corresponding *E*-Δ8-desaturation product sphingenine (d18:1$^{\Delta 8E}$) (Fig. 1A, table S1). Then the FA profile of free Cers was analysed, which covers the comprehensive Cer composition of complexed SLs as the biosynthetic intermediates (Markham and Jaworski, 2007; Ishikawa et al., 2016). Targeted multiple

reaction monitoring of Cers in *O. tauri* crude extract revealed that C16:0 was the major FA, and C14:0 and C18:0 were minor components (1-2 mol% of total Cer) (Fig. 1B). Only trace amounts of very-long-chain fatty acids C22:0 and C24:0 were detected (~0.1 mol% of total Cer) and other FA derivatives were under detection limits. It thus appears that *O. tauri* Cers display a limited diversity with *E*-Δ8-desaturation being the only modification detected in our conditions.

Detailed characterization of *O. tauri* SL headgroups was carried out according to the methodology of Ishikawa et al. (Ishikawa et al., 2016) (Fig. 2, Fig. S1). In land plants and some algae, GIPCs and GlyCers are known as the major GSLs (Mamode Cassim et al., 2020). GSLs provide the specific product ions (i.e., ceramide and LCB moieties) in MS/MS analysis under a positive ionization mode. Based on the ceramide composition of *O. tauri* (Fig. 1), the total lipid extract from *O. tauri* was applied to the precursor ion scanning using the fragment of d18:1 LCB (*m*/*z* 264.3, $[LCB-2H_2O+H]^+$ for Cer and mono-glycosylated SLs) and d18:1-16:0 ceramide (*m*/*z* 520.5, $[Cer-H_2O+H]^+$ for more complexed SLs) (Fig. 2, Table S1). The MS^2 analysis provided the *m*/*z* of putative precursor species 538.5, 714.6 and 890.6 for LCBs (Fig 2A) and 714.5, 890.6, 1052.6, 1214.7, and 1376.7 for Cers (Fig 2B). The *m*/*z* 538.5 corresponds to d18:1-c16:0 Cer, and thus the larger fragments were estimated as GSLs. The differences between the *m*/*z* 890.6, 1052.6, 1214.7 and 1376.7 are Δ162, which can be unambiguously attributed to hexose (Hex) attachments (Fig. 2C). There are therefore up to three Hex residues at the terminal end of GSLs. In addition, the differences Δ176 (*m*/*z* 890.6 from 714.6 and *m*/*z* 714.6 from 538.5) and Δ194 (*m*/z 714.6 from 520.5) can be attributed to hexuronic acid (HexA, without or with H_2O, respectively). Thereof, up to two HexA residues are attached to the base of the glycosyl chain (Fig. 2C). Vice Versa, the product ion scanning of the predicted precursor ions supported the glycan structure (Fig S1). However, highly glycosylated molecules are often difficult to be unambiguously determined by ESI-MS, as multiple deglycosylated fragments are detected via in-source fragmentation. We therefore assessed the above results by further performing targeted MS^2 analysis coupled with a reverse-phase HPLC separation. This enabled us to detect four separate peaks in the LC chromatograms, which were assigned to Cer, HexACer, Hex_2HexA_2Cer, and Hex_3HexA_2Cer (Fig. 2D). The chromatograms obtained with MRM settings for $HexA_2Cer$ and $HexHexA_2Cer$ were overlapped with that for Hex_2HexA_2Cer, and the peak at 9.7 min of retention time was also detected in the windows for Cer and HexACer but not for Hex_3HexA_2Cer where a distinct peak was detected at 9.2 min, indicating that the

overlapped peaks are Hex_2HexA_2Cer and its in-source fragmentation products. Note that neither (G)IPC nor GlcCers were detected by the scanning and targeted analysis that has been successively developed for the GSLs in land plants (Ishikawa et al., 2016).

In summary, *O. tauri* has five classes of GlyCers and does not contain GIPCs. The diversity of Cers moieties of SLs is limited to two major species i.e. d18:0/C16:0 and $d18:1^{\Delta 8E}$/C16:0, while glycosyl moieties are composed to up to five residues and have the remarkable peculiarity of containing hexuronic acids at the base of the glycosidic chain. The only eukaryotic GSLs that contain hexuronic acids and that might be polyglycosylated described so far are GIPCs. Hexuronic acid-containing polyglycosylated Cers were only reported from the proteobacteria genus *Sphingomonas* (Kawahara et al., 2000).

Characterisation of the sphingolipid Δ8 desaturase from *O. tauri*

As Δ8-desaturation of LCB chain was the only modification detected, we aimed at gaining insight into the regulation and possibly functional significance of SLs Δ8-desaturation in *O. tauri*. Temperature has been shown to modify the composition of GSLs in plants and cold to impair the growth of plants mutants defective for LCBs Δ8-dessaturation (Chen et al., 2012; Nagano et al., 2014; Zhou et al., 2016). We therefore aimed at investigating the effect of temperature on sphingolipid composition and in particular on LCB unsaturation in *O. tauri*.

Phylogenetic analysis of Δ8-sphingolipid desaturase candidates

Our previous work enabled us to identify all the desaturases (Des) in *O. tauri* and to identify a putative homologue of SLD8 (genomic accession Ot15g01140) (Degraeve-Guilbault et al., 2020). Similarly as fatty-acid Δ4, Δ5 and Δ6 -desaturases, Δ8-sphingolipid desaturases have a Cytochrome b5 (CytB5) domain fused at the N terminus (Nt) of the protein that has co-evolved with the desaturase domain (Gostincar et al., 2010). It is worth recalling here that SLD8s only occur in plants and fungi, and further that plant FA Δ6-Des only occur in a few 18:3n-6 producing plant species. *O. tauri* and related species have the peculiarity of displaying animal-like Δ6-Des that uses Acyl-CoA as substrate rather than lipids but branch separately from their animal counterparts (Domergue et al., 2005; Gostincar et al., 2010). In addition, we recently discovered the first plastidial Δ6-Des (Degraeve-Guilbault et al., 2020). We therefore conducted two phylogenetic analyses of the *O. tauri* SLD8 homologue considering firstly SLD8

182 from various organismsincluding taking care to include SLD8s with functionally assessed
183 activity (Fig. 3A), and secondly Mamiellales CytB5-fused desaturases (Fig. 3B) (Tonon et al.,
184 2005; Oura and Kajiwara, 2008; Li et al., 2016; Degraeve-Guilbault et al., 2020).
185 The phylogenetic analysis run with SLD8s from various organisms shows that the
186 Mamiellales clade, together with its sister clade (PP= 0.70) containing Charophyte sequences,
187 sits basally (PP = 1.00) to a robust clade (PP = 1.00) containing characterised SLD8s from
188 Bryophytes and higher plants (Fig. 3A, Fig. S2). The *Nymphaea thermarum* sequence defines
189 the monocot/eudicot separation, as expected following the Paleoherb hypothesis (Doyle and
190 Donoghue, 1993; Igersheim and Endress, 1998). Considering sequences from the distant
191 microalgal lineage SAR, sequences cluster together, with the exception of the two diatoms
192 species *Nitzschia inconspicua* and *Thalassiosira pseudonana*.–The only cryptophyte in the
193 analysis (*Guillardia theta*), has possibly destabilised the analysis (PP = 0.55). *T. pseudonana*
194 SLD8 is the only SAR sequence that has been functionally characterised to date and was shown
195 to exclusively produce *E* isomer (Tonon et al., 2005). Bayesian phylogenetic analysis using
196 amino acid (AA) sequences of all CytB5-fused desaturases from Mamiellales shows that the
197 putative *O. tauri* SLD8 AA sequence robustly clusters (posterior probability PP = 1.00) with
198 other Mamiellales putative SLD8 and is related (posterior probability PP = 0.75) to the clade
199 of Mamiellales plastidial Δ6-Des (Fig. 3B) (Degraeve-Guilbault et al., 2020). The acyl-CoA Δ6-
200 Des clade robustly (1.00) clusters basally to the clade containing both the SLD8 and the
201 plastidial Δ6-Des.
202 In summary, OtSLD8 robustly clusters with plant SLD8 and further SLD8, pΔ6-Des and
203 acyl-CoA-Δ6-Des clades of Mamiellales species are robustly related suggesting a common
204 ancestor in Mamiellophyceae

205 *Subcellular localization of SLD8 candidates*

206 In order to complete the AA sequence of the NCBI/JGI accessions, we searched for
207 additional possible start codons 5' upstream of, and in frame with, the annotated nucleotide
208 sequence (Fig. S3). Putative start codons 5' upstream of the automatically annotated start
209 codons occurred for *O. tauri*, *Ostreococcus* sp. RCC809 and *Micromonas pusilla*. For *O. tauri*,
210 we successfully amplified the corresponding sequence from cDNA. From subcellular
211 localisation prediction (PredAlgo) fair to high scores for chloroplastidic target peptide (cTP)
212 were obtained for all Mamiellales sequences exception made of *Bathycoccus prasinos* (Tardif

et al., 2012). In particular, the 33 AA extended OtSLD8 sequence displayed a cTP score of 3.11 over 5 (Fig. S3). We therefore considered a short version and a long version of SLD8 for subsequent analyses (short-SLD8 and long-SLD8 thereafter). The subcellular localisation of both SLD8 version was investigated expressing Cterminal-YFP-fused proteins in *Nicotiana benthamiana* as previously done for other *O. tauri* FA-desaturases (Degraeve-Guilbault et al., 2020; Degraeve-Guilbault et al., 2021). The short-SLD8 was unambiguously ER located while the long-SLD8 localised at chloroplasts (Fig. 3). These results suggest that two versions SLD8 might exist in *O. tauri* one being located in the ER the other to the chloroplast.

Expression in yeast

Heterologous expression of *OtSLD8* in the yeast *Saccharomyces cerevisiae* was achieved to assess the substrate specificity of SLD8 (Table 1, Fig. S4). Both short- and long- *SLD8* versions were expressed in different strains available from previous studies, along with *SLD1* from *Arabidopsis thaliana* as positive control and an empty vector as negative control. *S. cerevisiae* strains allowed to test specific substrate: the wild-type strain provides t18:0, the *sur2Δ* mutant d18:0 and the *sur2Δ* expressing the LCB Δ4 desaturase gene of *Komagataella pastoris* provides d18:1$^{\Delta 4E}$ (Haak et al., 1997; Ternes et al., 2002). Further note that the *pGAL1* inducible system was used in addition to the constitutive expression system (promoter *PGK1)* as expression of *long-SLD8* slowed-down the growth of yeasts. As previously reported, AtSLD1 showed comparable unsaturation efficiency for sphinganine (d18:0) and 4-hydroxysphinganine (t18:0) and produced both *Z* and *E* isomers (Fig. S4). In contrast, OtSLD8 displayed a clear preference for dihydroxylated substrate as both SLD8 versions produced about five times more product from sphinganine than from 4-hydroxysphinganine (Table 1). Only *E* stereoisomers were produced (Fig. S4). Both saturated and monounsaturated dihydroxylated substrates (d18:0, d18:1$^{\Delta 4E}$) appeared equally well accepted by OtSLD8 while SLD1 had a clear preference for 4-sphingenine (d18:1$^{\Delta 4E}$).These results are consistent with the LCB analysis from *O. tauri* and support that d18:1$^{\Delta 8E}$ is the only d18:0 desaturation product in the alga.

In summary, *O. tauri* SLD8 , displayed a clear preference for di-hydroxylated C18 LCBs, whether they were saturated or ∆4-unsaturated, and produced exclusively *E*-isomers. These features are strongly reminiscent of the distant diatom SLD8 homologue TpdesB (Tonon et al., 2005).

Search for additional desaturase activity

O. tauri has the capacity of producing a peculiar fatty acid 18:5$^{\Delta3,6,9,12,15}$ which is commonly found in species from the SAR supergroup (Degraeve-Guilbault et al., 2017). C18:5 is recognised as a hallmark of galactolipids (plastidial lipids) and is assumed to be derived from the activity of a previously unidentified Δ3-desaturase using 18:4$^{,\Delta6,9,12,15}$ as substrate. The first plastidial Δ6-desaturases (pΔ6-Des) that we have recently discovered do not appear to produce this compound (Degraeve-Guilbault et al., 2020). Although it seemed unlikely that a sphingolipid desaturase accepts glycerolipids as substrates, we wanted to investigate whether SDL8 could display additional enzymatic activity in particular when co-expressed with pΔ6-Des (Fig. 5) (Li et al., 2016). We therefore co-expressed SLD8 with OtΔ6-Des in the heterologous host *N. benthamiana.* The reasoning behind this experiment is, on the one hand, that homo and heterodimerisation of glycerolipid desaturases have been reported (Lou and Shanklin, 2010; Lou et al., 2014) and, on the other hand, that some glycerolipid desaturases display labile regiospecificity (Hastings et al., 2001; Heilmann et al., 2004; Li et al., 2010; Bláhová et al., 2022; Kabeya et al., 2023).

The *long-SLD8* was expressed together with each of the *pΔ6-Des (pΔ6-Des1 and pΔ6-Des2*) (Fig. 5A) and the *Short-SLD8* with the ER *acyl-CoA-Δ6-Des* (Fig. 5B) (Degraeve-Guilbault et al., 2020). Consistently with previous report, overexpression of *Δ6-Des* in *N. benthamiana* resulted in the production of 18:3n-6 and 18:4n-3 from 18:2n-6 and 18:3n-3, respectively with the greatest conversion observed for pΔ6-Des1 (Fig. 5A). However, expression of OtSDL8 alone or in combination with other OtΔ6-Des did not result in other noticeable changes in the fatty acid profiles of *N. benthamiana*.

Effect of temperature on SLD8 expression

Standard temperature of *O. tauri* culture is 20°C. We have previously identified 24°C and 14°C as the best temperatures for studying glycerolipid dynamics and desaturase expression as a function of temperature (Degraeve-Guilbault et al., 2021). Cells synchronised by light/dark cycles and acclimatised to 14°C or 24°C were either warmed up or cooled down 3-4 hours after the light was switched on. This time was chosen to correspond to the peak of SLD8 expression, which occurs in the morning.(Monnier et al., 2010) (Fig. S5).

SLD8 transcript abundance was monitored at 24°C and 14°C in cells acclimated (at least 15 generations), 30 min and 4 hours after chilling and warming (Fig. 6). The transcript level was unambiguously higher at 14°C than at 24°C, and following the temperature change adjusted within 30 minutes and remained similar to the control 4 hours later (Fig. 6).

SLD8 functional analyses in *O. tauri*

We next wanted to gain insight into SLD8 function in the native host. Genetic transformation of *O. tauri* remains a challenging technique with low yields and, although gene replacement by homologous recombination has been reported, it requires in-depth screening of hundreds of clones (Corellou et al., 2009; Lozano et al., 2014). Valid approaches for gene silencing or CRISPR-Cas9 that could circumvent this bottleneck have not yet been developed. Therefore, the overexpression strategy currently remains the most accessible method for carrying out functional analyses in *O. tauri*; it has previously proven successful to gain insight into FA-desaturase functions (Degraeve-Guilbault et al., 2020; Degraeve-Guilbault et al., 2021).

The long-SLD8 was cloned into the pOtOx-Luc vector and SLD8 overexpressors (SLD8-OEs) were selected according to their luminescent level (see methods) (Fig. 7A). The promoter driving the overexpression is the high affinity phosphate transporter from *O. tauri* (HAPT or Pho4). It has a high activity compared to most other endogenous promoters SLD8 promoter included (Fig. S6A, B) (Degraeve-Guilbault et al., 2020). SLD8 transcript levels were further assessed for seven of SDL8-OEs and one transgenic containing the empty vector (EV) as negative control (Fig. 7B, Fig. S6C). For most of the lines, SLD8 transcript levels were about five times higher than in control. FA analyses indicated that the FA-profile SLD8 transgenics was undistinguishable from WT or EV (Fig. 7C).

LCB unsaturation was compared between 14°C and 24°C in 4 independent SLD8-OEs and 4 independent control lines (EVs). Interestingly, LCB Δ8-unsaturation at 24°C in control lines was about half of that at 14°C (87.71%±0.19 and 47.59 % to ±3.38, respectively). In contrast, LCB Δ8-unsaturation at 24°C in SLD8-OEs reached a level close to the EVs at 14°C (86.53% ±2.39) and was even higher at 14°C (93.61%±0.87) (Fig. 7D). These results indicate that 1) LCB Δ8-unsaturation is inversely correlated to temperature 2) expressing SLD8 from the HAPT promoter dramatically enhances LCB Δ8-unsaturation at 24°C.

Effect of temperature and of SLD8 overexpression on sphingolipids

To determine whether temperature and/or Δ8 unsaturation level affect the relative amount of GSL species, we carried out the detailed analysis of SL in four independent SLD8-OE lines (Fig. 8A, Fig. S7) and four independent control (EV) lines acclimated to either 14°C or 24°C (Fig. 8B, Fig. S7). To obtain an overall trend, the values for the individual lines of each type were averaged (Fig. 8C-F). Temperature and *SLD8* overexpression had a major impact on the SL unsaturation while the impact on SL relative amounts was more subtle.. At both temperatures, the relative amounts of Cers and mono-GlyCers were slightly lower in SLD8-OE than in EV, while those of tetra- and penta-GlyCers were higher (Fig. 8C). Overall, the same variations were observed in SLD8-OEs and EVs as a function of temperature, with lower levels of Cers and tetra-GlyCers and higher levels of mono-GlyCers and penta-GlyCers at 14°C than at 24°C (Fig. 8D).

LCB Δ8-unsaturation occurred in all SLs. Penta-GlyCers displayed the highest unsaturation rate reaching 85% at 24°C, whereas mono-GlyCers were the least unsaturated with only 20% of unsaturation at 24°C (Fig. 8E). For control lines, the unsaturation rate roughly doubled at 14°C in all classes but penta-GlyCers, whose unsaturation was increased to 93%. In SLD8-OEs, the unsaturation rate of SLs at 24°C was closely related to that of EVs at 14°C and further increased at 14°C suggesting that a post-transcriptional mechanism might limit the activity of the overexpressed SLD8 at 24°C (Fig. 8A, B, E). As mentioned above, although the relative abundance of SLs was slightly altered in SLD8-OEs, the variations as a function of temperature followed a similar trend as in control. This suggests that LCB-unsaturation had a minor effect on SL relative abundance.

To summarise: 1) although SLD8-OEs and EVs display slight differences in the relative abundance of SL classes, variations between 24°C and 14°C display a similar trend 2) LCB Δ8-unsaturation is increased in all SL classes at 14°C as well as in SLD8-OEs.

Effect of temperature on SLD8-OE growth, cell-size and fluorescence

In order to gain insight into the physiological significance of SL Δ8-unsaturation as a function of temperature, flow cytometry was used to monitor cell parameters of selected SLD8 OEs and EV along a growth kinetics at 24°C, 14°C and after switching the temperature from 24°C to 14°C and reversed (Fig. 9, Fig. S8, Fig. S9, Table S2).Cell parameters included cell

density, cell-size (FSC parameter) and structure (SSC parameter) as well as chlorophyll fluorescence. Cells acclimated to 24°C and 14°C were sub-cultured and allowed to reach exponential growth. On the second day of culturing, triplicate cultures were transferred to either lower or higher temperature 4 hours after light on, while control triplicate were kept at the original temperature (Fig. S9A-D).

Cell growth was similar between SLD8-OEs and EV in all conditions (Fig. 9A, Fig. S8). The generation time was significantly lower at 24°C compared to 14°C and slightly slowed-down upon chilling. Interestingly for both SLD8-OEs and EV, FSC, SSC (Fig. 9B, C, Fig. S8E) cell parameters (Fig. 9D, E, Table S2) were overall higher at 24°C than at 14°C suggesting that cell-size, cell structure and chlorophyll fluorescence all positively correlated with temperature. Chilling and warming triggered the progressive adjustment of these parameters that reached values close to those of acclimated cells after 7 to 8 days of culture (Fig. 9B-E, Fig. S9A-B). However, the FSC, SSC and red fluorescence parameters were overall lower in SLD8-OEs, the probabilities of a significant difference with EV being higher at 24°C than at 14°C (Fig. 9B-E, Fig. S9). In particular, the size of SLD8-OEs at 24°C was closely related to that at 14°C (Fig. 9B, C, Fig. S9E, Table S2) yielding a reduced size-ratio between 24°C and 14°C in SLD8-OEs compared to EV (Fig. S9F). Upon warming, SLD8-OEs cell-size appeared to increase though to a lesser extent than in EV, letting the differences between SLD8-OEs and EV progressively emerge along the growth kinetics (Fig. 9B). Conversely, chilling resulted in abolishing the cell-size/structure differences between SLD8-OE and EV within 24 hours after the temperature-shift. Although a similar trend occurred for chlorophyll fluorescence (Fig. 9D, E, Fig. S9D), values in cells acclimated at 14°C remained significantly lower in SLD8-OEs.

Altogether, these results suggest that overexpressing SLD8 impairs cell-size adjustment at 24°C and correlates with a lower chlorophyll content at both temperatures.

Sphingolipid genes

Based on our results and further retrieval of *O. tauri* SLs related genes homologues, we propose a SL pathway in *O. tauri* (Fig. 10, Fig. S10). Concerning LCB/ceramide modification enzymes, no SLD4 orthologue could be retrieved from the *O. tauri* genome, though putative homologues were found in *Micromonas* species. No homologue of fatty acid hydroxylase (AtFAH1) was found in any Mamiellales species except *Bathycoccus prasinos*. These results are

consistent with LCB Δ8-unsaturation being the only SL modification detected in *O. tauri*. However, although we did not detect a t18:0, a putative homologue of LCB C4-hydroxylase was found in *Ostreococcus* species and *Micromonas commoda*. Surprisingly, a putative homologue of the LCB C9-methyltransferase, usually found in fungi, also occurred in all Mamiellales species. Putative LCB/ceramide-P phosphatase homologues were also retrieved (not represented).

Homologues of enzymes central to SL synthesis that were easily identified include serine palmitoyl transferase (SPT) and ceramide synthase (CS), the latter being more closely linked to the SAR lineage. As regards to the glycosylceramide synthase (GSC), putative *A. thaliana* homologues were found in *Bathycoccus* and *Micromonas* but not in *Ostreococus* species. However, we found putative homologues of the bacterial glucuronosylceramide and galacturonylceramide synthases in *O. tauri* as well as in other Mamiellales species (Okino et al., 2020). Finally, the search for enzymes involved in the synthesis of GIPC (IPC-synthase, inositolphosphoryl ceramide synthase) proved unsuccessful in agreement with the lack of GIPCs in *O. tauri*.

DISCUSSION

While the literature widely reports an inverse correlation between temperature and the unsaturation of glycerolipid FAs, this is not the case for the LCBs constituting SLs (Nagano et al., 2014; Holm et al., 2022). As a result, the hypothesis that unsaturated FAs counteract the rigidification of membranes in the cold has become widespread (Ernst et al., 2016). This hypothesis, which is already debatable in the case of polyunsaturated fatty acids (PUFAs), is not, in our opinion, applicable to LCBs (Degraeve-Guilbault et al., 2021). Noteworthy, double bond in the *trans* configuration does not lower the melting temperature of the FA as much as that in the *cis* configuration. Nevertheless, *trans* unsaturation that prevails in LCBs are supposed to increase the physical distance between the hydrophobic core of SLs and other lipids. LCB desaturation could therefore be involved in the precise and/or local regulation of membrane properties, contributing, for example, to the dynamics of microdomains (Fernandes et al., 2016; Huby et al., 2020). As in most organisms LCB Δ8-unsaturation is either a prerequisite for other modifications and/or impacts on the channelling of Cer backbones towards the synthesis of different classes of GSLs (Jiang et al., 2021; Haslam and Feussner, 2022). *Candida albicans* SLD8 knocked-out (KO) mutants have provided the first evidence that

LCB Δ8-unsaturation might be related to low temperature acclimation (Oura and Kajiwara, 2008). SLD8 KOs displayed a lower growth rate at 10°C than at the control temperature (30°C). However, mutants also exhibited a slower filamentation independently of the temperature. Similarly, the disruption of SLD8 in *Aspegillus nidulans* resulted in defects in growth and morphology, including the absence of conidial development, which appear to be unrelated to temperature (Fernandes et al., 2016). It is noteworthy that LCB Δ8-desaturation is a prerequisite for LCB C9-methylation in fungi, making it difficult to separate the respective contributions of these modifications. Finally, *Arabidopsis* SLD8 KOs, whose cold growth is impaired, not only lack Δ8-unsaturated LCBs, but also experience a 50% reduction in the quantity of GlcCer, while GIPCs are increased (Chen et al., 2012).

We showed here that LCB Δ8-trans-monounsatutation is the only modification occurring in *O. tauri* unique GSLs. Temperature tightly regulated LCB Δ8-desaturation while having only slight effects on GSLs content. Our results further suggest that increasing LCB Δ8-unsaturation by SLD8 overexpression correlates with a lower chlorophyll content and impairs cell-size increase at 24°C. The following sections will discuss in more details the peculiarity of *O. tauri* GSLs and the temperature dependent regulation of LCB Δ8-desaturation.

O. tauri SL polar heads are reminiscent of bacterial glycosylceramides

O. tauri lacks GIPCs but displays unique GlyCers comprising hexuronic acid residues and polyglycosylated heads. Betaine lipids are phosphate–free glycerolipids that have been proposed as substitutes for phospholipids in microalgae . Although speculative, it is possible that the peculiar GlyCers discovered in O. tauri, which apart from phosphate, have characteristics of GIPCS, are adaptive substitutes for GIPCs in phosphate-poor environments. The occurrence of GlyCers in *O. tauri* is consistent with the prevalence of GlyCers in marine microalgae (Stonik and Stonik, 2018). However, as in plants, the glycosyl moieties of microalgal SLs usually consisted of only one sugar residues that is further a neutral sugar (glucose, galactose). Glycosyl moieties consisting of di to trisaccharidic residues were however reported from some centric diatoms species (*Thalassiosira pseudonana* and *Skeletonema*) while a monosaccharide sialic acid SL head group was identified in the haptophyte *Emiliania huxleyi* (Fulton et al., 2014; Stonik and Stonik, 2018). Interestingly, acidic poly-GlyCers consisting of glucuronic or galacturonic acids and up to three additional hexose residues are characteristic

of proteobacteria from the genus *Sphingomonas* and homologues of the bacterial glucuronylceramide synthase were found in Mamiellales (Kawahara et al., 1991; Kawahara et al., 2000; Okino et al., 2020). These hexuronyl containing SLs serve to replace lipopolysaccharide lacking in the outer membrane of sphingomodacae. Microalgae from the Mamiellophyceae class have no cell wall but characteristic scales with a spider-web structure. *Ostreoccoccus* and the closely related genus *Micromonas* are exceptions and lack scales. Biochemical analyses of scales from microalgae formerly referred to as "prasinophytes" (paraphyletic group including Mamiellophyceae) showed that they are composed primarily of acidic polysaccharides containing unusual 2-keto sugar acids (Becker et al., 1991; Moreau et al., 2012). Similarly as for acidic GlyCers functionally replacing LPS in bacteria, acidic GlyCers could be a substitute for scales in *O. tauri*. Possibly acidic GlyCers could replace GIPCs in a phosphoate poor In this regard, it would be interesting to investigate the conservation of GSLs in Mamiellales, and in particular, to know whether *Bathycoccus prasinos* which, in contrast to *Ostreococcus* and *Micromonas* genera, displays GSLs containing hexuronic acid.

Ceramide modification is restricted to Δ8-desaturation and highly regulated by temperature

Contrasting with the originality of SL head-group, Cer backbone diversity is limited to d18:0/C16:0 and d18:1^{8E}/C16:0 species. Di-hydroxylated LCBs are largely prevalent in marine microalgae and phytosphingosine has only been reported from the terrestrial green alga *Chlamydomonas reinhardtii*, (Kong et al., 2015; Stonik and Stonik, 2018). The absence of tri-hydroxylated LCBs in *O. tauri* is therefore not surprising. However, microalgal species analysed so far comprised a more diversified Cer pool composed of di to tri -desaturated LCBs and hydroxylated and/or desaturated FAs of different chain lengths (Li et al., 2017; Stonik and Stonik, 2018). By comparison, *O. tauri* Cer backbone appeared very simple.

More interestingly, the unsaturation level of LCB Δ8-unsaturation correlates closely with temperature, with the unsaturation level of the major GSLs at 24°C being about half of the unsaturation level at 14°C and significantly reduced from 93% to 85% in Hex_3HexA_2Cers. At the best of our knowledge, such a tight temperature-dependent regulation of LCB unsaturation has never been reported, as of the time of writing. The idea that LCB Δ8-desaturation is involved in the cold response is largely based on experiments by Chen and

collaborators who showed that the *Arabidopsis sld1 sld2* double mutant which totally lacks Δ8-unsaturated LCB, exhibited advanced chlorosis and reduced root growth after prolonged exposure to cold. (Chen et al., 2012). However, it should be remembered that in WT, the relative level of LCB unsaturation is not altered by cold exposure, leading to the proposal that "unsaturated LCBs may be required for basic cold resistance rather than for tolerance induced after cold exposure" (Nagano et al., 2014). Similarly, no correlation between LCB unsaturation and cold hardiness/acclimation emerged from the detailed lipidomic analysis of *Arabidopsis* natural accessions displaying various freezing tolerance (Degenkolbe et al., 2012). Finally, from survey of t18:1^{8} *Z* and *E* isomers in chilling resistant/sensitive plants it was proposed that the t18:1^{8} *trans* isomer might correlate with freezing tolerance (Imai et al., 1997; Kawaguchi et al., 2000). Variations of t18:1^{8} *Z* and *E* isomers as a function of temperature in a given species has however never been reported. To our knowledge, the only slight changes in LCB unsaturation as a function of temperature were recently evidenced in tobacco pollen tubes where the relative amount of Δ4-unsaturated LCBs, and to a much lesser extent Δ8-unsaturated LCBs, was slightly reduced by heat stress (Krawczyk et al., 2022).

Impairing temperature-dependent regulation LCB unsaturation correlates with defect of cell-size upon warming

In *O. tauri* WT, the relative abundances of LCB unsaturation and SLD8 transcript varied in unison, being about twice higher at 14°C than at 24°C. Consistently, overexpression of SLD8 significantly increased the LCB unsaturation level at 24°C, erasing the differences observed in control cell between 14°C and 24°C in all SL classes. Moreover, cell-size and chlorophyll fluorescence exhibited significant variations as a function of temperature being higher at 24°C than at 14°C in control cells (EV). Interestingly, SLD8-OE remained as small at 24°C as at 14°C and exhibited a lower chlorophyll fluorescence than the control at both 24°C and 14°C. As the lack of increase in cell-size at 24°C correlates with a marked increase in LCB unsaturation in SLD8-OEs, it is tempting to speculate that the decrease of LCB unsaturation is required for increasing *O. tauri* cell volume at 24°C. Knowing whether SLD8 knock-outs show an inverse phenotype would help to support this hypothesis. However, it should be emphasised that in our case the level of overexpression is moderate, which minimises the possibility of an indirect effect. The main criticism of the overexpression strategy is the risk of titration of protein

partners or cofactor that may be involved in processes other than those under study. The fusion of CytB5 in SLD8 alleviates the possibility of CytB5 titration and the only SLD8 partner identified to date in plants, is the Bax-inhibitor 1 which has no homolog in Mamiellophyceae (Nagano et al., 2014).

The temperature-dependent variations of *O. tauri* cell-size and chlorophyll b (chl b) fluorescence observed in our conditions are consistent with previous works examining the impact of temperature on marine phytoplankton physiology. Typically, phytoplankton acclimated to low temperatures show a photophysiology comparable to that of high-light-acclimated phytoplankton, with low levels of cellular chlorophyll a (chl a) (Geider, 1987; Maxwell et al., 1994; Stramski et al., 2002). Photophysiologty adaptation of *O. tauri* from 20°C to 24°C includes the increases of both chl a and chl b, light harvesting capacity and electron transport, all likely to support the enhanced growth rates at higher temperatures (Kulk et al., 2012). The cell-size increase between 14°C and 24°C observed in our study is consistent with a recent report showing that *O. tauri* cells acclimated to 33°C had a fourfold higher cell volume than at 20°C (Barton et al., 2023). The temperature-size rule (TSR) describes an inverse relationship between organism size and environmental temperature. *O. tauri* cell-size variations therefore illustrates a case of reverse-TSR also described for the diatom *Thalassiosira pseudonana* (Schaum et al., 2018). In the ocean, temperature and nutrients are strongly anticorrelated and small cells, due to a higher surface-area-to-volume ratio, are believed to be better cope with nutrient diffusion limitation (Marañón et al., 2012). It is also possible that *O. tauri* grown at 14°C have a smaller chloroplast. Since the chloroplast occupies 50% of the *O. tauri* cell volume, variations of the chloroplast size are likely to reverberates on the overall cell-size (Henderson et al., 2007).

Our results support the notion that LCB Δ8-unsaturation is related to low temperature acclimation in *O. tauri*. However, the mechanisms involved and whether the failure to adapt chlorophyll content and cell-sizecell-size are an epiphenomenon remains to be clarified.

METHODS

Chemicals

Chemicals were purchased from Merck, Sigma Chemical (St. Louis, MO, USA) and Wako (Tokyo, Japan) when not otherwise stated. Lipids used as internal standards were purchased

from Avanti Polar Lipids (Alabaster, AL, USA). Internal standards were prepared according to Markham et al. (2007).

Sequences and phylogeny analyses

Sequences were obtained from NCBI. SLD8 from Mamiellophyceae species were manually checked for completion of nucleaotide sequences as reported previously for other desaturases (Degraeve-Guilbault et al., 2020; Degraeve-Guilbault et al., 2021). Briefly, open reading frame (ORF) encompassing a start methionine upstream of the annotated start codon were taken into account. Target peptides were predicted from PredAlgo (Tardif et al., 2012). Desaturase sequences alignment was performed using Snapgene trial version (Clustal omega).

Phylogenetic analyses used OtSLD8 as query to retrieve homologs from as many taxa as possible. The first dataset produced contained hundreds of sequences with the most populated phylum in plants. A subset of plant sequences was chosen, which encompassed sequences of proteins that have been functionally characterised (Li et al., 2016). The subset was then back-BLASTed in all the major repositories (NCBI, Ensembl, JGI) and a new dataset containing SAR and fungal protein was produced. The dataset was visualised in BioEdit v7.0.5.3 computer program then aligned and curated using the MAFFT v7.407_1 (Katoh and Standley, 2013)and BMGE v1.12_1 (Criscuolo and Gribaldo, 2010) tools implemented in NGphylogeny.fr (Lemoine et al., 2019). The final alignment included 46 sequences and 326 residues including gaps. Two independent Metropolis-Coupled Markov chain Monte Carlo (MCMCMC) analyses were used to infer Bayesian phylogenetic relationships using MrBayes v3.2.7_0 software (Ronquist et al., 2012) implemented in NGphylogeny.fr. Each analysis involved one cold and three warm chains. The number of generations was set at 2.000.000 and with a sampling frequency every 500 generations and a burn-in fraction set at 0.25, i.e. the first 500.000 tree topologies were discarded to stabilise the analyses. The parameters of the likelihood model was set to ‘mixed’ hence the algorithm was allowed to jump from one model implemented in the software to the other according to dataset. A gamma distribution probability was set. Once the analysis completed, the outcome was saved in the Nexus format and then visualised in FigTree v1.4.4 to set colours.

The histidine boxes previously identified were aligned following the clades produced in the Bayesian inference and were used to feed WebLogo3 (Crooks et al., 2004) online tool to produce the sequence logos in Figure 1.

Biological material and cultures

O. tauri cells (clonal isolate from OtH95) were grown under 18:6 photoperiod in artificial sea-water (ASW) NaCl 4.1 $x10^{-1}$ M, KCL $8x10^{-3}$ M, $MgCl_2.6H_2O$ $3.2x10^{-2}$ M, $CaCl_2$ $2.7x10^{-3}$ M, Tris–HCl 5mM pH 7.6; supplemented with $NaNO_3$ 8.82. 10^{-4} M, NaH_2PO_4 $3.62.10^{-5}$, and F/2 components without silicium (ncma.bigelow.org/algal-recipes). Cultures were grown in incubator-shaker (New Brunswick Innova 42R) with constant agitation (80 RPM) under white light (75 mmol photons m^{-2} s^{-1}, 6 X T8 fluorescent bulbs 15 Watt each (Sylvania Gro-Lux). In standars conditions *O. tauri* was grown at 20°C. The tempratures 24°C and 14°C have been previously identified as the best temperatures to investigate difference in desaturase expresssion and lipid unsaturation and *O. tauri* were acclimated to these temperatures for at least 3 su-culturing rounds (about 15 generations) (Degraeve-Guilbault et al., 2021). For screening of FA of *O. tauri* transgenics, cells were grown in T25 aerated culture flasks (Sartstedt, Nümbrecht, Germany). Phosphate (NaH_2PO_4) was reduced from 35 µM to 5 µM to allow the expression of transgenes under the high affinity phosphate transporter promoter. Bacteria associated to *O. tauri* were reduced to less than 5% using centrifugation (1500 g, 5 min, RT) and antibiotic treatment (vancomycin 1 mg/mL, 4 days followed by G418 0.5 mg/ml, 4 days). Survey of bacterial population was achieved by flow cytometry as previously reported (Degraeve-Guilbault et al., 2017).

Flow cytometry

Cells were fixed with 0.5 % glutaraldehyde (Grade II) and analysed on a flow Cytometer (Partec CyFlow Space FACS). Refractory parameters are forward scatter (FSC), and side scatter (SSC) reflecting cell-size and structure, respectively. Chlorophyll fluorescence arises from the excitation of chlorophyll a at 488 nm and its emission in the red channel. *O. tauri* cell were discriminated based on the red fluorescence and counted.

568 Temperature shift

569 Cells were acclimated to 24°C and 14°C for at least 3 weeks (through 3 subculturing).
570 During this period, the cell density was regularly adjusted to ensure consistency between
571 conditions and transgenics. In the final round of subculturing, a low phosphate medium was
572 used to induce the full expression of transgenes. By the time 0 of the experiment, each batch
573 was subcultured in 6 independent flasks and allowed to recover for 62 hours before the
574 temperature shift. Sampling of 1 mL of culture was achieved along the growth kinetics and
575 fixed cells were analysed within 6 h.

576 Cloning strategy

577 PCR amplifications of DES ORF were achieved using Q5® Polymerase by two-step PCR on cDNA
578 matrix (5'-GGGCCCATGGCGTCGTCGGTGGGCG ATGCGCGCCGCGACGTC-3'.and 5'-
579 CTAGTCGCCCCGCTCCCAGAC-3'), which encompassed the restriction sites ApaI for cloning in
580 pOtox-Luc (Moulager et al., 2010). The amplified fragment was subcloned in pGEM®-T Easy
581 (Promega, Madison, WI, US) and sequenced (Genwiz, Leipzig, Germany). Cloning using
582 Gateway® system was performed according to manufacturer instructions (pDONR 221,
583 pK7W2G2D or pK7YWG2 for *N. benthamiana*). Sequences for either the long or the short
584 version of SLD8 were amplified from the SLD8 sequence cloned in pGEMT with primer
585 encompassing the extension AttB1 and AttB2 extension. Codon-optimised sequences
586 (GenScript Biotech, Netherlands) were used for overexpression in *S. cerevisiae*.

587 RNA and cDNA preparation and quantitative RT-PCR analysis

588 RNeasy-Plus Mini kit (Qiagen, Hilden, Germany) was used for RNA purification; DNase I
589 was used to remove contaminating DNA (DNA-free kit, Invitrogen, Carlsbad, USA) and cDNA
590 obtained using the reverse transcription iScript™ supermix kit (Bio-Rad, Hercules, CA, USA).
591 Primers used for qPCR were (5'-CCCTTCGCGGAAAAGAATGG-3'.and 5'-
592 GCTTGAGCGTTCGAAACACC -3'). Real-time RT quantitative PCR reactions were performed in a
593 CFX96™ Real-Time System (Bio-Rad) using the GoTaq® qPCR Master mix (Promega, Madison,
594 WI, USA). Bio-Rad CFX Manager software was used for data acquisition and analysis (version
595 3.1, Bio-Rad). Ct method was used to normalise transcript abundance with the references

ACTprot2 (Actin protein-related 2). PCR efficiency ranged from 95 to 105%. Technical triplicate were used, and at least two independent experiments were achieved.

Genetic transformation

O. tauri electroporation was adapted from (Corellou et al., 2009). In brief, 1.5×10^9 cells were collected by centrifugation, resuspended in 80µl 1M sorbitol, mixed with 5µg of linearised pOtOX-Luc vector and transferred into a 2mm wide electroporation cuvette. Electroporation was performed using Gene Pulser Xcell Electroporator (Bio-Rad), field strength 7 kV/cm, resistor 600 Ω, capacitor 25 µF. Transformants were selected on semi-solid agarose (0.21% final concentration) containing 1.5 mg/mL of G418. The pOtOX-Luc vector, in addition to the HAPT promoter driving the expression of transgene further contains the luciferase gene under the CCA1 promoter. Luciferase expression allows to readily select the best overexpressors. High luminescence indicates high luciferase gene expression and consequently best genetic environment for the activity of the HAPT promoter driving the expression of SLD8.

S. cerevisiae was transformed by the standard LiAc/SS carrier DNA/PEG method (Gietz and Schiestl, 2007) using pEG423 vector. Control lines were transformed with of empty vectors. *N. benthamiana* leaves from five-week old plants were infiltrated with *Agrobacterium tumefaciens* previously transformed by electroporation; the p19 protein to minimise plant post-transcriptional gene silencing (PTGS) was used in all experiments (Shah et al., 2013). Briefly, *A. tumefaciens* transformants were selected with antibiotics (gentamycin 25 µg/mL with spectinomycin 100 µg/mL or kanamycin 50 µg/mL). *Agrobacterium* transformants were grown overnight, diluted to an OD_{600} of 0.1 and grown to an OD_{600} of 0.6-0.8. Cells were re-suspended in 5 mL sterilie water for a final OD_{600} of 0.4 and 0.2 for overexpression and subcellular localization experiments, respectively and 1 mL was agroinfiltrated. Plants were analysed 2 and 5 days after *Agrobacterium* infiltration for subcellular localization experiments and for overexpression, respectively.

Lipid analysis

For all organisms, FA analyses and for *O. tauri* further lipid analysis were achieved as previously reported (Degraeve-Guilbault et al., 2017).

To obtain total LCB composition, lyophilised *O. tauri* cells or fresh yeast cells were directly hydrolyzed in 10% barium hydroxide/dioxane (1:1) for 24 h at 110°C. After cooling, the solvent was vigorously mixed with 0.5 volumes of diether ether and 4% sodium sulfate and the upper phase was collected and evaporated. LCB was derivatised with NBD-F and analysed by LC-MS/MS according to the previous report (Ishikawa et al., 2014) with the MRMs shown in Table S1.

Total sphingolipid extract was prepared and analysed as previously described with some modifications (Ishikawa et al., 2016; Ukawa et al., 2022). In brief, lyophilised cells were homogenised by vigorous shaking with glass beads in 1-butanol/methanol (2:1). The homogenate was mixed with 0.6 voluimes of 1 N KOH and kept for 30 minutes at 50°C. The mixture was acidified with HCl and phase-separated by adding 1-butanol. The upper layer was collected and dried under vacuum. The residue was dissolved in THF/methanol/water containing 0.1% formic acid and injected to LC-MS/MS (LCMS-8030, Shimadzu GLC). For MS/MS analysis of GSL structures, the sample was directly injected into MS under a flow of methanol/isopropanol/acetonitrile (1:1:1) containing 5 mM ammonium formate. Precursor ion scanning analysis was performed with product ion of m/z 264.3 (LCB) or 520.5 (Cer) and a range of precursor ion scan between *m*/*z* 250 to 1800. Targeted MS/MS analysis was performed using the MRMs shown in Table S1. The solvent system and MS parameters were according to Ishikawa et al. (2016).

Confocal microscopy

Live cell imaging was performed using a Leica SP5 confocal laser scanning microscopy system (Leica, Wetzlar, Germany) equipped with Argon, DPSS, He-Ne lasers, hybrid detectors, and 63× oil-immersion objective. *N. benthamiana* leaf samples were mounted on a glass slide using drop of water and covered with a coverslip. Fluorescence was measured using excitation/emission wavelengths of 488/490-540 nm for chlorophyll, 488/575- 610 nm for YFP. Co-localisation images were taken using sequential scanning between frames. Experiments were performed using strictly identical confocal acquisition parameters (*e.g.* laser power, gain, zoom factor, resolution, and emission wavelengths reception), with detector settings optimized for low background and no pixel saturation.

654 Stastistics

655 Statistical analyses were performed using Microsoft Excel. A Student's test was
656 employed to compare two datasets, while a Tukey test to compare multiple datasets
657 simultaneously (multiple pair-wise comparison, p-value < 0.05). Compact letter display was
658 used to clarify the output. Variables that that do not have statistically different means from
659 one another will share the same letter. (Schlattmann and Dirnagl, 2010). Groups sharing the
660 same letter are statistically indistinguishable and belong to the same set, while groups that
661 exhibit detectable differences are assigned distinct letters representing different sets. When
662 a group is labeled with more than one letter, it signifies an 'overlap' between sets of
663 groups.Table 1

		Unsaturation %				
		OtSLD8			AtSLD1	
		Short		Long		
Substrate	Product	Pro-PGK1	Pro-GAL1	Pro-GAL1	Pro-PGK1	Pro-GAL1
t18:0	t18:1(Δ8)	5.5 ± 0.7	5.7 ± 0.8	7.5 ± 1.0	21.0 ± 0.4	19.8 ± 0.9
d18:0	d18:1(Δ8)	24.6 ± 0.8	32.6 ± 1.1	21.1 ± 0.2	28.2 ± 0.5	24.2 ± 1.0
d18:1(Δ4)	d18:2(Δ4,8)	23.1 ± 1.2	*NE	*NE	77.6 ± 0.4	*NE

664 **Table.1. OtSLD8 LCB desaturase activity in S. cerevisiae.**

665 The wild-type strain (W303-1A), sur2Δ (BY4741), and sur2Δ expressing the Δ4 sphingolipid
666 desaturase of Komagataella pastoris were used to determine the desaturation activity on
667 t18:0, d18:0, and d18:14E, respectively. The percent of unsaturation was calculated by the
668 formula (product)/(substrate + product)*100. Means and standard deviations are shown
669 (n=3).*NE: not examined due to the same Pro-GAL1 plasmid used for expression of
670 OtSLD8/AtSLD1 and Pichia Δ4 desaturase.

671 **ACKNOWLEDGMENTS AND FUNDINGS**

672 We would like to thank M. Michaud for his advice on the organisation of the manuscript and
673 A. Calame for proofreading the english language. Routine lipid analyses were performed at
674 the Metabolome Facility of Bordeaux-MetaboHUB (ANR-11-INBS-0010). Imaging was
675 performed at the Bordeaux Imaging Center, member of the national infrastructure France

BioImaging. The yeast expression vector pGK423 was provided by the National Bioresource Project (NBRP, Japan).

Fundings: Université de Bordeaux- grant SB2: 2017–2019, project acronym PICO-FADO, Université de Bordeaux grant Emergence 2019, project acronym TOTOX.

AUTHOR CONTRIBUTIONS

AA and FC performed the phylogenetic analyses. FC performed most of the experimental work and analyses) related to *O. tauri* (cultures, cytometry analyses, cloning, transformation, FAMES analysis, RT-qPCR) and wrote the MS. FD performed the work and analyses on *N. benthamiana* (cloning, agro-transformation, and FAMES analysis). TI performed the experimental work and analyses related to desaturase expression in yeast and *O. tauri* sphingolipid characterisation and wrote the corresponding sections. All authors contributed to the article and approved the submitted version.

FIGURE LEGENDS

Figure 1. Analysis of total LCBs and of free ceramides from *O. tauri*.

A. LC-MS/MS profile of total LCBs liberated from whole cells of *O. tauri*. LCBs were analysed as the NBD-derivatives by LC-MS/MS and the MRM chromatograms of the five major species conservatively observed in plants are shown at the same scale of absolute intensities of MS signal intensities. **B**. Fatty-acids of free ceramides. Free ceramides composed of d18:0 or d18:1 LCB and one of various fatty acids were detected by LC-MS/MS by the targeted MRM mode. The MRM transitions are shown in Table S1.

Figure 2. Characterisation of *O. tauri* GSLs.

A. Precursor ion scanning using the product ion corresponding to d18:1 LCB. **B**. Precursor ion scanning using the product ion corresponding to d18:1-16:0 Cer. **C**. Assignment of the detected *m*/*z* to GSLs containing HexA and Hex residues. **D**. Targeted LC-MS/MS chromatogram of *O. tauri* GSLs. Four separate peaks were determined as below; 1, Hex_3HexA_2Cer; 2, Hex_2HexA_2Cer; 3, HexACer; 4, free Cer. The MRMs used were combination of molecular ions ($[M+H]^+$) and the major product ions for each species, i.e., *m*/*z* 264.3 ($[d18:1\text{-}2H_2O+H]^+$) for Cer, 520.5 ($[Cer\text{-}H_2O+H]^+$) for HexACer, and 538.5 ($[Cer+H]^+$) for longer GSLs as determined by the product ion scanning (Fig S1).

Figure 3. Phylogenic trees of the putative Δ8-sphingolipid desaturases from *O. tauri*.

The trees were drawn to scale in substitutions per site (scale bar on the figure). Posterior Probabilities (2.000.000 generations) lower than 1.00 are indicated by the nodes. Vertical bars indicate taxonomic assignment, also visualised by brench colors. A. Bayesian phylogenetic tree of SLD8s. The preference of the enzyme to catalyse the *E*- or *Z*-isomer is indicated for some species (bold) (Tonon et al 2005, Oura et al 2008, Li et al 2016). B. Figure 3. Bayesian phylogenetic tree of Mamiellales CytB5-fused desaturases. Posterior Probabilities (2.000.000 generations) greater than 0.95 are not reported, the others are indicated by the nodes.

Figure 4. Sub-cellular localisation of *O. tauri* sphingolipid D8-desaturase short and long versions in *Nicotiana benthamiana*.

Confocal images of *Nicotiana benthamiana* leaves transiently transformed with OtSLD8-YFP short and long versions. Images were taken 2 days post infiltration. Left, YFP signal; Right, merged of YFP signal and chlorophyll autofluorescence. Bars = 20µm.

Figure 5. Fatty-acid profile of *N. benthamiana* expressing SDL8 alone and together with D6-desaturases.

The anti-silencing protein p19 was used in all infiltrations. **A**. The long-SLD8 (plastid located) was expressed alone and together with the plastidial D6 desaturases pD6-Des1 and pΔ6-Des2. The number of replicate is indicated. **B**. The short version of SLD8 (ER located) was expressed alone and together with the ER Acyl-CoA-D6-Des (ACoA-Δ6-Des) (n=3). Means and standard errors are shown.

Figure 6. Effect of temperature on SLD8 expression.

Exponentially growing cells were shifted from 24°C to 14°C and reversed while control cells were maintained at the initial temperatures. Cells were harvested 0.5 and 4 h after the temperature shift. Means and standard deviations of technical triplicate are shown. Experiment was repeated twice.

Figure 7. Selection and lipidic analysis of SLD8 overexpressors.

Transgenics are labelled 15-n for SLD8 and EV for the empty vector. **A.** Luminescence of SLD8 transgenics. The Potos-Luc vector carries the luciferase under the CCA1 promoter allowing the selection of lines according to their luminescent level. The line EV3 containing the empty vector (v3 in Fig. S4C) was chosen as negative control for lipid analysis because it produces as much luminescence as SLD8-OEs (Fig. S4C). Means and standard deviation of technical triplicate are shown. **B.** SLD8 relative transcript levels in selected luminescent lines.

C. Fatty-acid profiles of SLD8 overexpressing lines. **D.** LCB unsaturation rate in control lines (grey) and SLD8 overexpressing lines (blue). Means and standard deviations of culture triplicate are shown. Values were compared among the different transgenics according to Tukey test at $p < 0.05$ and groups with the same letter are not detectably different.

Figure 8. Sphingolipid contents and unsaturation rates in control and SLD8 overexpressing lines as a function of temperature.

Four individual lines where cultivated in triplicate for each, negative controls (EV1,EV2,EV3,EV4, open colored symbols) and SLD8-OEs (15-5, 15-8, 15-10, 15-11 plain colored symbols). Cells acclimated at 24°C or at 14°C were collected at the end of exponential growth for analysis. **A-B**. Correlation between sphingolipid unsaturation rate and relative content in individual transgenic lines, control lines (EVs, A), SLD8-OEs (B). Means and standard deviations of independent triplicate are shown. Unsaturation rate is d18:1/(d18:0+d18:1) ×100 (%). **C**. Relative amount of sphingolipids in EVs and SLD8-OEs at 14°C and 24°C. **D**. Ratio of relative amount between 14°C and 24°C. **E**. Unsaturation rate in sphingolipid classes in EVs and SLD8-OEs at 14°C and 24°C. Errors bars for ratio z=x/y in D and F were calculated according to the error propagation rule $Dz=z\sqrt{(Dx/x)2+(Dy/y)2}$. C-F. Averages of the values from the 4 triplicates of EV lines (n=12) and SLD8-OE lines (n=12) are shown, errors bars are SD. Stastistical significances were calculated within each SL class using the Tukey test in C and E ($p < 0.05$), groups with the same letter are not detectably different, and using the pair-wise Student's t-test) in D and F ($p < 0.05$, ns is not significant).

Figure 9. Cellular parameters of SLD8-OEs and control lines along growth kinetics in different temperature conditions.

SLS8-OEs (15-5, 15-11) and negative control (EV) acclimated to 24°C or 14°C were grown in light/dark cycles (white and black boxes). After 62 hours of culture, one part was transferred from 24°C to 14°C (24°C>14°C) and from 14°C to 24°C (14°C>24°C) (dotted lines), while the other part was left at the initial temperature. **A**. Generation times in exponential growth after temperature change. The Tukey test was applied to all lines and conditions ($p < 0.05$) and groups with the same letter are not detectably different. Growth curves are available from Fig. S8. **B-E.** Evolution of FSC, i.e. cell-size at 24°C (B,C) and red fluorescence, i.e. chlorophyll b (D,E) in cells acclimated or transferred to 24°C (B,D) and in cells acclimated or transferred to 14°C (C,E). Means an SD from independent triplicate cultures are shown. Statistical significance by pairwise t-test between EV and SLD8-OE lines in each condition (*, $p < 0.1$; **,

$p < 0.05$; ***, $p < 0.001$), absence of label corresponds to non significant values. Vertical dotted lines represent the time of warming (red) and chilling (blue). Evolution of the SSC parameter and complementary representations are available from Fig S9.

Fig. 11. Sphingolipid pathway in *O. tauri*.

Enzymes involved in the metabolic step are indicated and corresponding genomic accession are indicated (italics). Homologues with E-values ≤ 9.00E-07 and query cover ≥ 41% are indicated in green boxes when obtained by blasting *A. thaliana* protein accessions and in pink box when obtained by blasting protein accessions from other organisms. Red frames highlight sphingolipids and SLD8 characterised in the present work. Activation and/or repression of SLD8 and LCB-D8-unsaturation by temperature and associated cell-size changes are schematised. Grey arrows represent unvalidated step. Details about blast results are provided in Fig. S10.

REFERENCES

Barton S, Padfield D, Masterson A, Buckling A, Smirnoff N, Yvon-Durocher G (2023) Comparative experimental evolution reveals species-specific idiosyncrasies in marine phytoplankton adaptation to warming. Global Change Biology **29:** 5261-5275

Becker B, Becker D, Kamerling JP, Melkonian M (1991) 2-KETO-SUGAR ACIDS IN GREEN FLAGELLATES: A CHEMICAL MARKER FOR PRASINOPHYCEAN SCALES1,2. Journal of Phycology **27:** 498-504

Bláhová Z, Franěk R, Let M, Bláha M, Pšenička M, Mráz J (2022) Partial fads2 Gene Knockout Diverts LC-PUFA Biosynthesis via an Alternative Δ8 Pathway with an Impact on the Reproduction of Female Zebrafish (Danio rerio). Genes (Basel) **13**

Chen M, Markham JE, Cahoon EB (2012) Sphingolipid Δ8 unsaturation is important for glucosylceramide biosynthesis and low-temperature performance in Arabidopsis. Plant J **69:** 769-781

Corellou F, Schwartz C, Motta JP, Djouani-Tahri el B, Sanchez F, Bouget FY (2009) Clocks in the green lineage: comparative functional analysis of the circadian architecture of the picoeukaryote ostreococcus. Plant Cell **21:** 3436-3449

Courties C, Vaquer A, RTrousselier M, Lautier J, Chrétiennot-Dinet M-J, Neveux J, Machado C (1994) Smallest eukaryotic organism. Nature **370:** 255

Criscuolo A, Gribaldo S (2010) BMGE (Block Mapping and Gathering with Entropy): a new software for selection of phylogenetic informative regions from multiple sequence alignments. BMC Evolutionary Biology **10:** 210

Crooks GE, Hon G, Chandonia JM, Brenner SE (2004) WebLogo: a sequence logo generator. Genome Res **14:** 1188-1190

Degenkolbe T, Giavalisco P, Zuther E, Seiwert B, Hincha DK, Willmitzer L (2012) Differential remodeling of the lipidome during cold acclimation in natural accessions of Arabidopsis thaliana. Plant J **72:** 972-982

Degraeve-Guilbault C, Bréhélin C, Haslam R, Sayanova O, Marie-Luce G, Jouhet J, Corellou F (2017) Glycerolipid Characterization and Nutrient Deprivation-Associated Changes in the Green Picoalga Ostreococcus tauri. Plant Physiology **173:** 2060-2080

Degraeve-Guilbault C, Gomez RE, Lemoigne C, Pankansem N, Morin S, Tuphile K, Joubès J, Jouhet J, Gronnier J, Suzuki I, Coulon D, Domergue F, Corellou F (2020) Plastidic Δ6 Fatty-Acid

Desaturases with Distinctive Substrate Specificity Regulate the Pool of C18-PUFAs in the Ancestral Picoalga Ostreococcus tauri. Plant Physiol **184:** 82-96

Degraeve-Guilbault C, Pankasem N, Gueirrero M, Lemoigne C, Domergue F, Kotajima T, Suzuki I, Joubès J, Corellou F (2021) Temperature Acclimation of the Picoalga Ostreococcus tauri Triggers Early Fatty-Acid Variations and Involves a Plastidial ω3-Desaturase. Front Plant Sci **12:** 639330

Derelle E, Ferraz C, Rombauts S, Rouze P, Worden AZ, Robbens S, Partensky F, Degroeve S, Echeynie S, Cooke R, Saeys Y, Wuyts J, Jabbari K, Bowler C, Panaud O, Piegu B, Ball SG, Ral JP, Bouget FY, Piganeau G, De Baets B, Picard A, Delseny M, Demaille J, Van de Peer Y, Moreau H (2006) Genome analysis of the smallest free-living eukaryote Ostreococcus tauri unveils many unique features. Proc Natl Acad Sci U S A **103:** 11647-11652

Domergue F, Abbadi A, Zahringer U, Moreau H, Heinz E (2005) In vivo characterization of the first acyl-CoA Delta6-desaturase from a member of the plant kingdom, the microalga Ostreococcus tauri. Biochem J **389:** 483-490

Doyle JA, Donoghue MJ (1993) Phylogenies and angiosperm diversification. Paleobiology **19:** 141-167

Ernst R, Ejsing CS, Antonny B (2016) Homeoviscous Adaptation and the Regulation of Membrane Lipids. J Mol Biol **428:** 4776-4791

Fernandes CM, de Castro PA, Singh A, Fonseca FL, Pereira MD, Vila TV, Atella GC, Rozental S, Savoldi M, Del Poeta M, Goldman GH, Kurtenbach E (2016) Functional characterization of the Aspergillus nidulans glucosylceramide pathway reveals that LCB Δ8-desaturation and C9-methylation are relevant to filamentous growth, lipid raft localization and Psd1 defensin activity. Mol Microbiol **102:** 488-505

Fulton JM, Fredricks HF, Bidle KD, Vardi A, Kendrick BJ, DiTullio GR, Van Mooy BA (2014) Novel molecular determinants of viral susceptibility and resistance in the lipidome of Emiliania huxleyi. Environ Microbiol **16:** 1137-1149

Geider RJ (1987) LIGHT AND TEMPERATURE DEPENDENCE OF THE CARBON TO CHLOROPHYLL a RATIO IN MICROALGAE AND CYANOBACTERIA: IMPLICATIONS FOR PHYSIOLOGY AND GROWTH OF PHYTOPLANKTON. New Phytologist **106:** 1-34

Gietz RD, Schiestl RH (2007) High-efficiency yeast transformation using the LiAc/SS carrier DNA/PEG method. Nat Protoc **2:** 31-34

Gostincar C, Turk M, Gunde-Cimerman N (2010) The evolution of fatty acid desaturases and cytochrome b5 in eukaryotes. J Membr Biol **233:** 63-72

Haak D, Gable K, Beeler T, Dunn T (1997) Hydroxylation of Saccharomyces cerevisiae ceramides requires Sur2p and Scs7p. J Biol Chem **272:** 29704-29710

Hannich JT, Umebayashi K, Riezman H (2011) Distribution and functions of sterols and sphingolipids. Cold Spring Harb Perspect Biol **3**

Haslam TM, Feussner I (2022) Diversity in sphingolipid metabolism across land plants. J Exp Bot **73:** 2785-2798

Hastings N, Agaba M, Tocher DR, Leaver MJ, Dick JR, Sargent JR, Teale AJ (2001) A vertebrate fatty acid desaturase with Delta 5 and Delta 6 activities. Proc Natl Acad Sci U S A **98:** 14304-14309

Heilmann I, Pidkowich MS, Girke T, Shanklin J (2004) Switching desaturase enzyme specificity by alternate subcellular targeting. Proc Natl Acad Sci U S A **101:** 10266-10271

Henderson GP, Gan L, Jensen GJ (2007) 3-D ultrastructure of O. tauri: electron cryotomography of an entire eukaryotic cell. PLoS ONE **2:** e749

Holm HC, Fredricks HF, Bent SM, Lowenstein DP, Ossolinski JE, Becker KW, Johnson WM, Schrage K, Van Mooy BAS (2022) Global ocean lipidomes show a universal relationship between temperature and lipid unsaturation. Science **376:** 1487-1491

Hopes A, Mock T Evolution of Microalgae and Their Adaptations in Different Marine Ecosystems. *In* Encyclopedia of Life Sciences, pp 1-9

Hopes A, Mock T (2015) Evolution of Microalgae and Their Adaptations in Different Marine Ecosystems. *In* Encyclopedia of Life Sciences, pp 1-9

Huby E, Napier JA, Baillieul F, Michaelson LV, Dhondt-Cordelier S (2020) Sphingolipids: towards an integrated view of metabolism during the plant stress response. New Phytologist **225:** 659-670
Igersheim A, Endress PK (1998) Gynoecium diversity and systematics of the paleoherbs. Botanical Journal of the Linnean Society **127:** 289-370
Imai H, Ohnishi M, Hotsubo K, Kojima M, Ito S (1997) Sphingoid base composition of cerebrosides from plant leaves. Bioscience, biotechnology, and biochemistry **61:** 351-353
Ishikawa T, Imai H, Maki KY (2014) Development of an LC-MS/MS method for the analysis of free sphingoid bases using 4-fluoro-7-nitrobenzofurazan (NBD-F). Lipids **49:** 295-304
Ishikawa T, Ito Y, Kawai-Yamada M (2016) Molecular characterization and targeted quantitative profiling of the sphingolipidome in rice. Plant J **88:** 681-693
Islam MN, Jacquemot MP, Coursol S, Ng CK (2012) Sphingosine in plants--more riddles from the Sphinx? New Phytol **193:** 51-57
Jiang C, Ge J, He B, Zeng B (2021) Glycosphingolipids in Filamentous Fungi: Biological Roles and Potential Applications in Cosmetics and Health Foods. Frontiers in Microbiology **12**
Kabeya N, Kimura K, Matsushita Y, Suzuki S, Nagakura Y, Kinami R, Noda H, Takagi K, Okamoto K, Miwa M, Haga Y, Satoh S, Yoshizaki G (2023) Determination of dietary essential fatty acids in a deep-sea fish, the splendid alfonsino Beryx splendens: functional characterization of enzymes involved in long-chain polyunsaturated fatty acid biosynthesis. Fish Physiol Biochem **49:** 425-439
Katoh K, Standley DM (2013) MAFFT Multiple Sequence Alignment Software Version 7: Improvements in Performance and Usability. Molecular Biology and Evolution **30:** 772-780
Kawaguchi M, Imai H, Naoe M, Yasui Y, Ohnishi M (2000) Cerebrosides in Grapevine Leaves: Distinct Composition of Sphingoid Bases Among the Grapevine Species Having Different Tolerances to Freezing Temperature. Bioscience, Biotechnology, and Biochemistry **64:** 1271-1273
Kawahara K, Moll H, Knirel YA, Seydel U, Zähringer U (2000) Structural analysis of two glycosphingolipids from the lipopolysaccharide-lacking bacterium Sphingomonas capsulata. Eur J Biochem **267:** 1837-1846
Kawahara K, Seydel U, Matsuura M, Danbara H, Rietschel ET, Zähringer U (1991) Chemical structure of glycosphingolipids isolated from Sphingomonas paucimobilis. FEBS Lett **292:** 107-110
Kong JN, Hardin K, Dinkins M, Wang G, He Q, Mujadzic T, Zhu G, Bielawski J, Spassieva S, Bieberich E (2015) Regulation of Chlamydomonas flagella and ependymal cell motile cilia by ceramide-mediated translocation of GSK3. Mol Biol Cell **26:** 4451-4465
Krawczyk HE, Rotsch AH, Herrfurth C, Scholz P, Shomroni O, Salinas-Riester G, Feussner I, Ischebeck T (2022) Heat stress leads to rapid lipid remodeling and transcriptional adaptations in Nicotiana tabacum pollen tubes. Plant Physiol **189:** 490-515
Kulk G, de Vries P, van de Poll WH, Visser RJW, Buma AGJ (2012) Temperature-dependent growth and photophysiology of prokaryotic and eukaryotic oceanic picophytoplankton. Marine Ecology Progress Series **466:** 43-55
Leliaert F, Smith DR, Moreau H, Herron MD, Verbruggen H, Delwiche CF, De Clerck O (2012) Phylogeny and Molecular Evolution of the Green Algae. Critical Reviews in Plant Sciences **31:** 1-46
Lemoine F, Correia D, Lefort V, Doppelt-Azeroual O, Mareuil F, Cohen-Boulakia S, Gascuel O (2019) NGPhylogeny.fr: new generation phylogenetic services for non-specialists. Nucleic Acids Research **47:** W260-W265
Li D, Moorman R, Vanhercke T, Petrie J, Singh S, Jackson CJ (2016) Classification and substrate head-group specificity of membrane fatty acid desaturases. Comput Struct Biotechnol J **14:** 341-349
Li SF, Zhang GJ, Zhang XJ, Yuan JH, Deng CL, Hu ZM, Gao WJ (2016) Genes encoding Delta(8)-sphingolipid desaturase from various plants: identification, biochemical functions, and evolution. J Plant Res **129:** 979-987
Li Y, Lou Y, Mu T, Ke A, Ran Z, Xu J, Chen J, Zhou C, Yan X, Xu Q, Tan Y (2017) Sphingolipids in marine microalgae: Development and application of a mass spectrometric method for global

structural characterization of ceramides and glycosphingolipids in three major phyla. Anal Chim Acta **986:** 82-94
Li Y, Monroig O, Zhang L, Wang S, Zheng X, Dick JR, You C, Tocher DR (2010) Vertebrate fatty acyl desaturase with Δ4 activity. Proc Natl Acad Sci U S A **107:** 16840-16845
Lou Y, Schwender J, Shanklin J (2014) FAD2 and FAD3 desaturases form heterodimers that facilitate metabolic channeling in vivo. J Biol Chem **289:** 17996-18007
Lou Y, Shanklin J (2010) Evidence that the yeast desaturase Ole1p exists as a dimer in vivo. J Biol Chem **285:** 19384-19390
Lozano JC, Schatt P, Botebol H, Verge V, Lesuisse E, Blain S, Carre IA, Bouget FY (2014) Efficient gene targeting and removal of foreign DNA by homologous recombination in the picoeukaryote Ostreococcus. Plant J **78:** 1073-1083
Mamode Cassim A, Grison M, Ito Y, Simon-Plas F, Mongrand S, Boutté Y (2020) Sphingolipids in plants: a guidebook on their function in membrane architecture, cellular processes, and environmental or developmental responses. FEBS Lett **594:** 3719-3738
Marañón E, Cermeño P, Latasa M, Tadonléké RD (2012) Temperature, resources, and phytoplankton size structure in the ocean. Limnology and Oceanography **57:** 1266-1278
Marin B, Melkonian M (2010) Molecular phylogeny and classification of the Mamiellophyceae class. nov. (Chlorophyta) based on sequence comparisons of the nuclear- and plastid-encoded rRNA operons. Protist **161:** 304-336
Markham JE, Jaworski JG (2007) Rapid measurement of sphingolipids from Arabidopsis thaliana by reversed-phase high-performance liquid chromatography coupled to electrospray ionization tandem mass spectrometry. Rapid Commun Mass Spectrom **21:** 1304-1314
Markham JE, Li J, Cahoon EB, Jaworski JG (2006) Separation and identification of major plant sphingolipid classes from leaves. J Biol Chem **281:** 22684-22694
Mashima R, Okuyama T, Ohira M (2019) Biosynthesis of long chain base in sphingolipids in animals, plants and fungi. Future Sci OA **6:** Fso434
Maxwell DP, Falk S, Trick CG, Huner N (1994) Growth at Low Temperature Mimics High-Light Acclimation in Chlorella vulgaris. Plant Physiol **105:** 535-543
Michaelson LV, Napier JA, Molino D, Faure J-D (2016) Plant sphingolipids: Their importance in cellular organization and adaption. Biochimica et biophysica acta **1861:** 1329-1335
Michaelson LV, Zauner S, Markham JE, Haslam RP, Desikan R, Mugford S, Albrecht S, Warnecke D, Sperling P, Heinz E, Napier JA (2009) Functional characterization of a higher plant sphingolipid Delta4-desaturase: defining the role of sphingosine and sphingosine-1-phosphate in Arabidopsis. Plant Physiol **149:** 487-498
Monnier A, Liverani S, Bouvet R, Jesson B, Smith JQ, Mosser J, Corellou F, Bouget FY (2010) Orchestrated transcription of biological processes in the marine picoeukaryote Ostreococcus exposed to light/dark cycles. BMC Genomics **11:** 192
Moreau H, Verhelst B, Couloux A, Derelle E, Rombauts S, Grimsley N, Van Bel M, Poulain J, Katinka M, Hohmann-Marriott MF, Piganeau G, Rouze P, Da Silva C, Wincker P, Van de Peer Y, Vandepoele K (2012) Gene functionalities and genome structure in Bathycoccus prasinos reflect cellular specializations at the base of the green lineage. Genome Biol **13:** R74
Moulager M, Corellou F, Vergé V, Escande ML, Bouget FY (2010) Integration of Light Signals by the Retinoblastoma Pathway in the Control of S phase Entry in the Picophytoplanktonic Cell Ostreococcus PLoS Genet
Nagano M, Ishikawa T, Ogawa Y, Iwabuchi M, Nakasone A, Shimamoto K, Uchimiya H, Kawai-Yamada M (2014) Arabidopsis Bax inhibitor-1 promotes sphingolipid synthesis during cold stress by interacting with ceramide-modifying enzymes. Planta **240:** 77-89
Okino N, Li M, Qu Q, Nakagawa T, Hayashi Y, Matsumoto M, Ishibashi Y, Ito M (2020) Two bacterial glycosphingolipid synthases responsible for the synthesis of glucuronosylceramide and α-galactosylceramide. J Biol Chem **295:** 10709-10725
Oura T, Kajiwara S (2008) Disruption of the sphingolipid Delta8-desaturase gene causes a delay in morphological changes in Candida albicans. Microbiology (Reading) **154:** 3795-3803

Ronquist F, Teslenko M, van der Mark P, Ayres DL, Darling A, Höhna S, Larget B, Liu L, Suchard MA, Huelsenbeck JP (2012) MrBayes 3.2: Efficient Bayesian Phylogenetic Inference and Model Choice Across a Large Model Space. Systematic Biology **61:** 539-542

Schaum CE, Buckling A, Smirnoff N, Studholme DJ, Yvon-Durocher G (2018) Environmental fluctuations accelerate molecular evolution of thermal tolerance in a marine diatom. Nature Communications **9:** 1719

Schlattmann P, Dirnagl U (2010) Statistics in experimental cerebrovascular research: comparison of more than two groups with a continuous outcome variable. J Cereb Blood Flow Metab **30:** 1558-1563

Shah KH, Almaghrabi B, Bohlmann H (2013) Comparison of Expression Vectors for Transient Expression of Recombinant Proteins in Plants. Plant molecular biology reporter **31:** 1529-1538

Sperling P, Zahringer U, Heinz E (1998) A sphingolipid desaturase from higher plants. Identification of a new cytochrome b5 fusion protein. J Biol Chem **273:** 28590-28596

Stonik VA, Stonik IV (2018) Sterol and Sphingoid Glycoconjugates from Microalgae. Mar Drugs **16**

Stramski D, Sciandra A, Claustre H (2002) Effects of temperature, nitrogen, and light limitation on the optical properties of the marine diatom Thalassiosira pseudonana. Limnology and Oceanography **47:** 392-403

Takakuwa N, Kinoshita M, Oda Y, Ohnishi M (2002) Isolation and characterization of the genes encoding delta(8)-sphingolipid desaturase from Saccharomyces kluyveri and Kluyveromyces lactis. Curr Microbiol **45:** 459-461

Tardif M, Atteia A, Specht M, Cogne G, Rolland N, Brugiere S, Hippler M, Ferro M, Bruley C, Peltier G, Vallon O, Cournac L (2012) PredAlgo: a new subcellular localization prediction tool dedicated to green algae. Mol Biol Evol **29:** 3625-3639

Ternes P, Franke S, Zahringer U, Sperling P, Heinz E (2002) Identification and characterization of a sphingolipid delta 4-desaturase family. J Biol Chem **277:** 25512-25518

Tonon T, Sayanova O, Michaelson LV, Qing R, Harvey D, Larson TR, Li Y, Napier JA, Graham IA (2005) Fatty acid desaturases from the microalga Thalassiosira pseudonana. Febs j **272:** 3401-3412

Ukawa T, Banno F, Ishikawa T, Kasahara K, Nishina Y, Inoue R, Tsujii K, Yamaguchi M, Takahashi T, Fukao Y, Kawai-Yamada M, Nagano M (2022) Sphingolipids with 2-hydroxy fatty acids aid in plasma membrane nanodomain organization and oxidative burst. Plant Physiol **189:** 839-857

Zhou Y, Zeng L, Fu X, Mei X, Cheng S, Liao Y, Deng R, Xu X, Jiang Y, Duan X, Baldermann S, Yang Z (2016) The sphingolipid biosynthetic enzyme Sphingolipid delta8 desaturase is important for chilling resistance of tomato. Sci Rep **6:** 38742

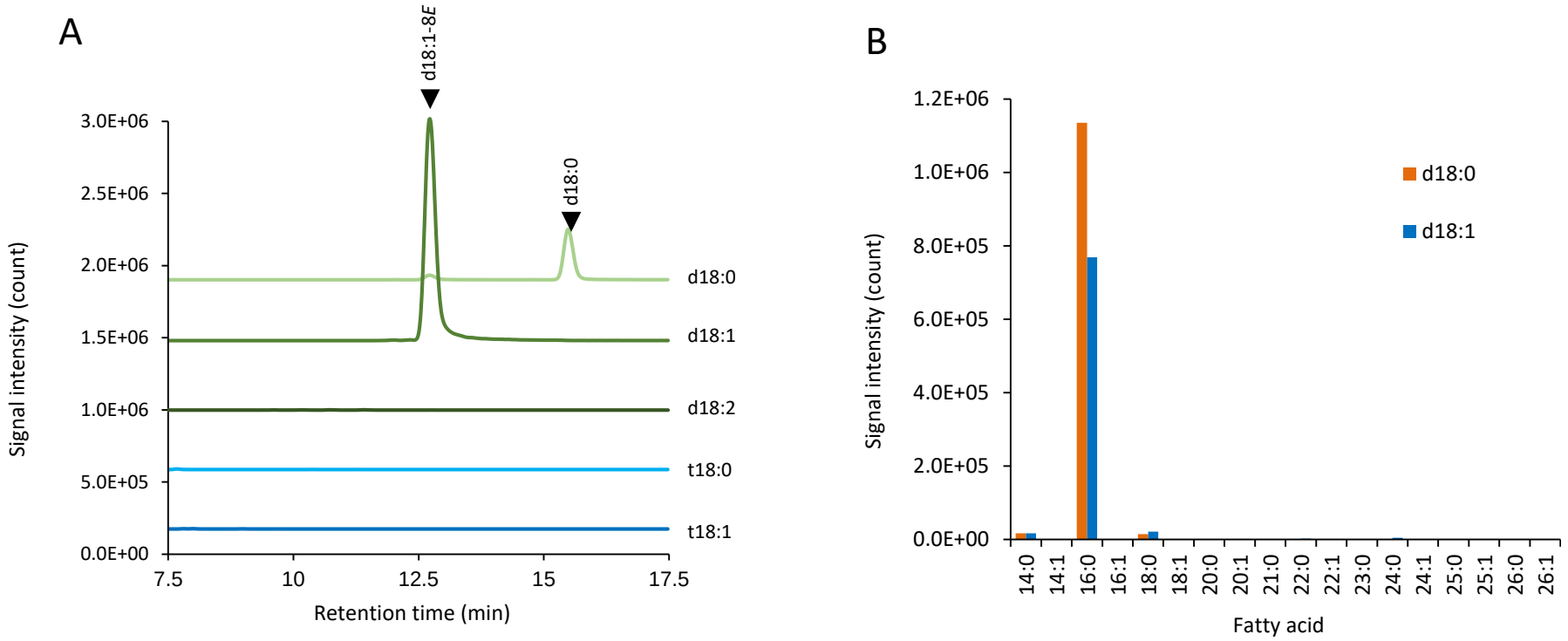

Figure 1. Analysis of total LCBs and of free ceramides from *O. tauri*.
A. LC-MS/MS profile of total LCBs liberated from whole cells of *O. tauri*. LCBs were analysed as the NBD-derivatives by LC-MS/MS and the MRM chromatograms of the five major species conservatively observed in plants are shown at the same scale of absolute intensities of MS signal intensities. **B**. Fatty-acids of free ceramides. Free ceramides composed of d18:0 or d18:1 LCB and one of various fatty acids were detected by LC-MS/MS by the targeted MRM mode. The MRM transitions are shown in Table S1.

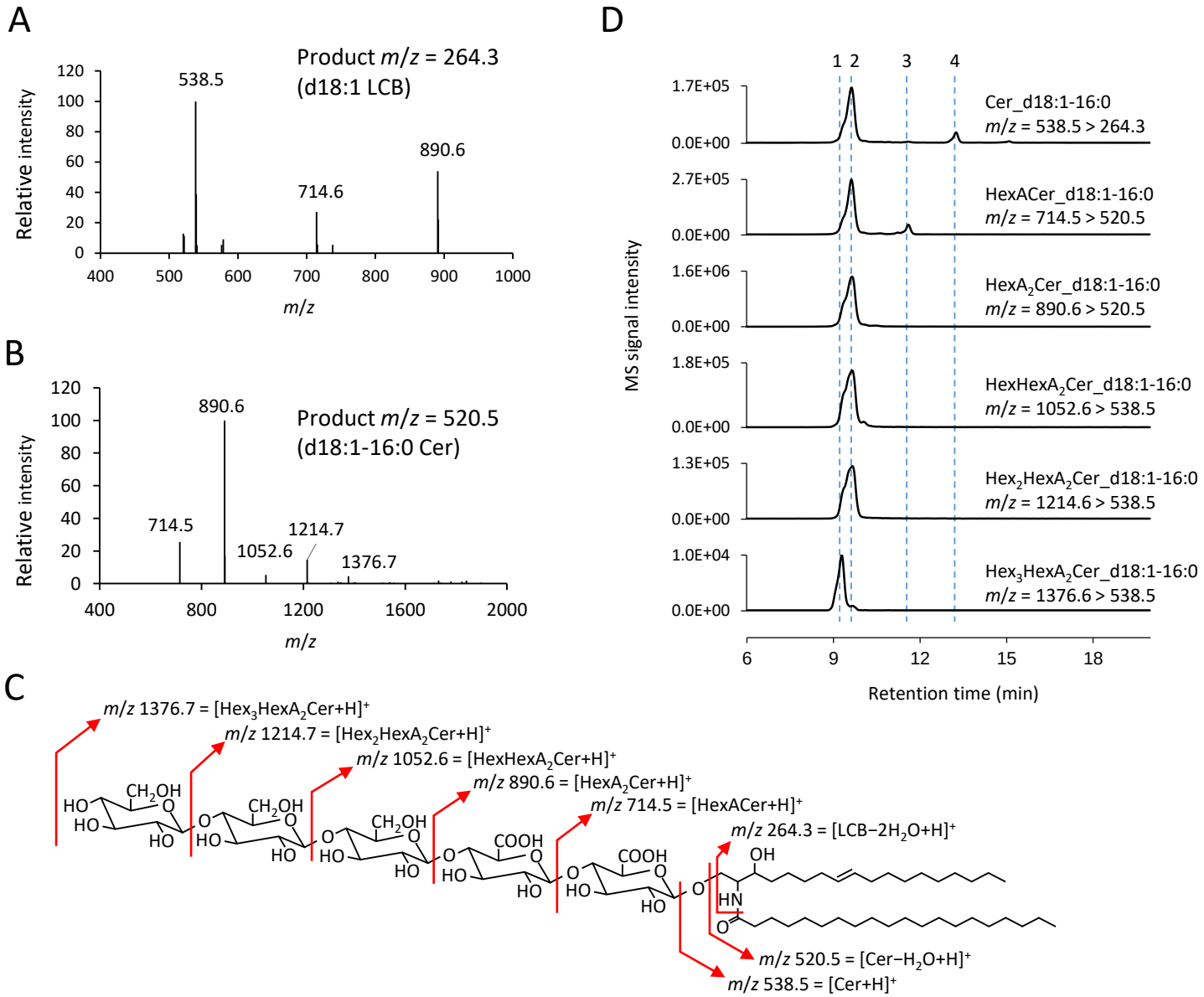

Figure 2. Characterisation of *O. tauri* GSLs.

A. Precursor ion scanning using the product ion corresponding to d18:1 LCB. **B**. Precursor ion scanning using the product ion corresponding to d18:1-16:0 Cer. **C**. Assignment of the detected *m/z* to GSLs containing HexA and Hex residues. **D**. Targeted LC-MS/MS chromatogram of *O. tauri* GSLs. Four separate peaks were determined as below; 1, Hex_3HexA_2Cer; 2, Hex_2HexA_2Cer; 3, HexACer; 4, free Cer. The MRMs used were combination of molecular ions ($[M+H]^+$) and the major product ions for each species, i.e., *m/z* 264.3 ($[d18:1\text{-}2H_2O+H]^+$) for Cer, 520.5 ($[Cer\text{-}H_2O+H]^+$) for HexACer, and 538.5 ($[Cer+H]^+$) for longer GSLs as determined by the product ion scanning (Fig S1).

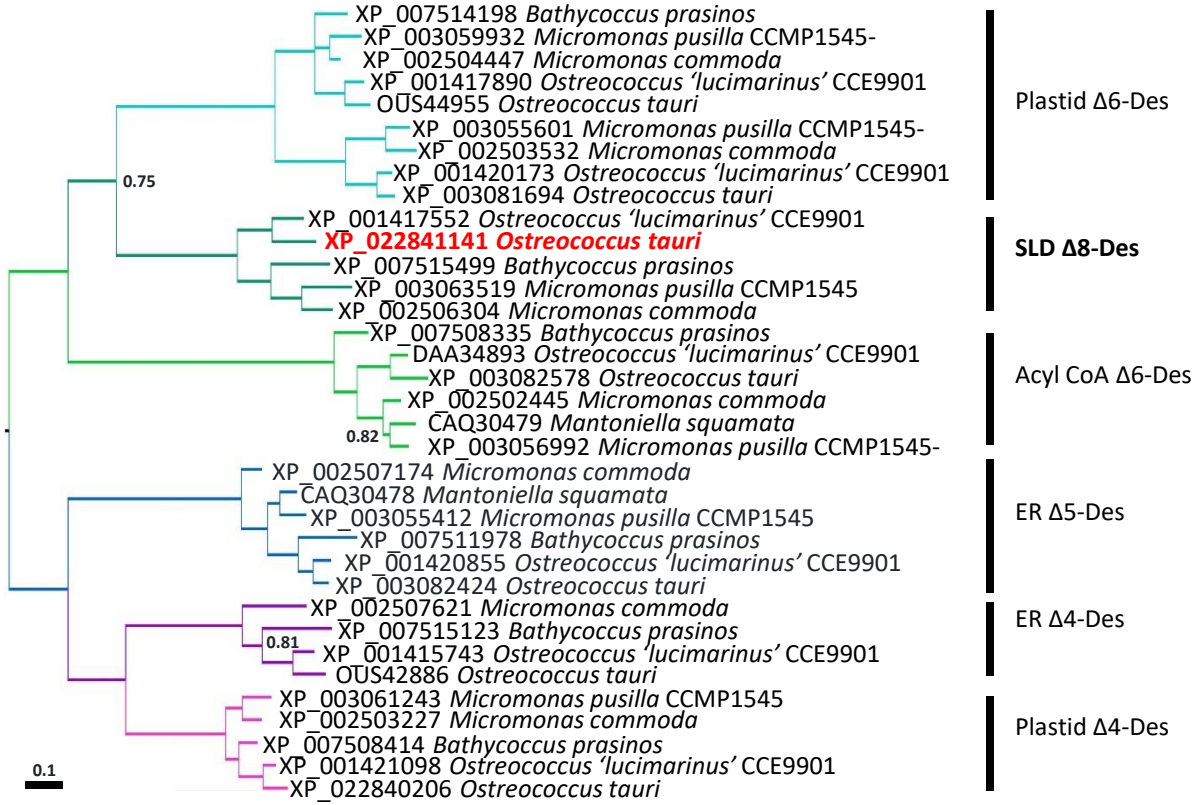

Figure 3. Bayesian phylogenetic tree of Mamiellales desaturases.
The tree was drawn to scale in substitutions per site (scale bar on the figure). Posterior Probabilities (2.000.000 generations) greater than 0.95 are not reported, the others are indicated by the nodes. Vertical bars indicate protein function. The *O. tauri* accession is highlighted in red

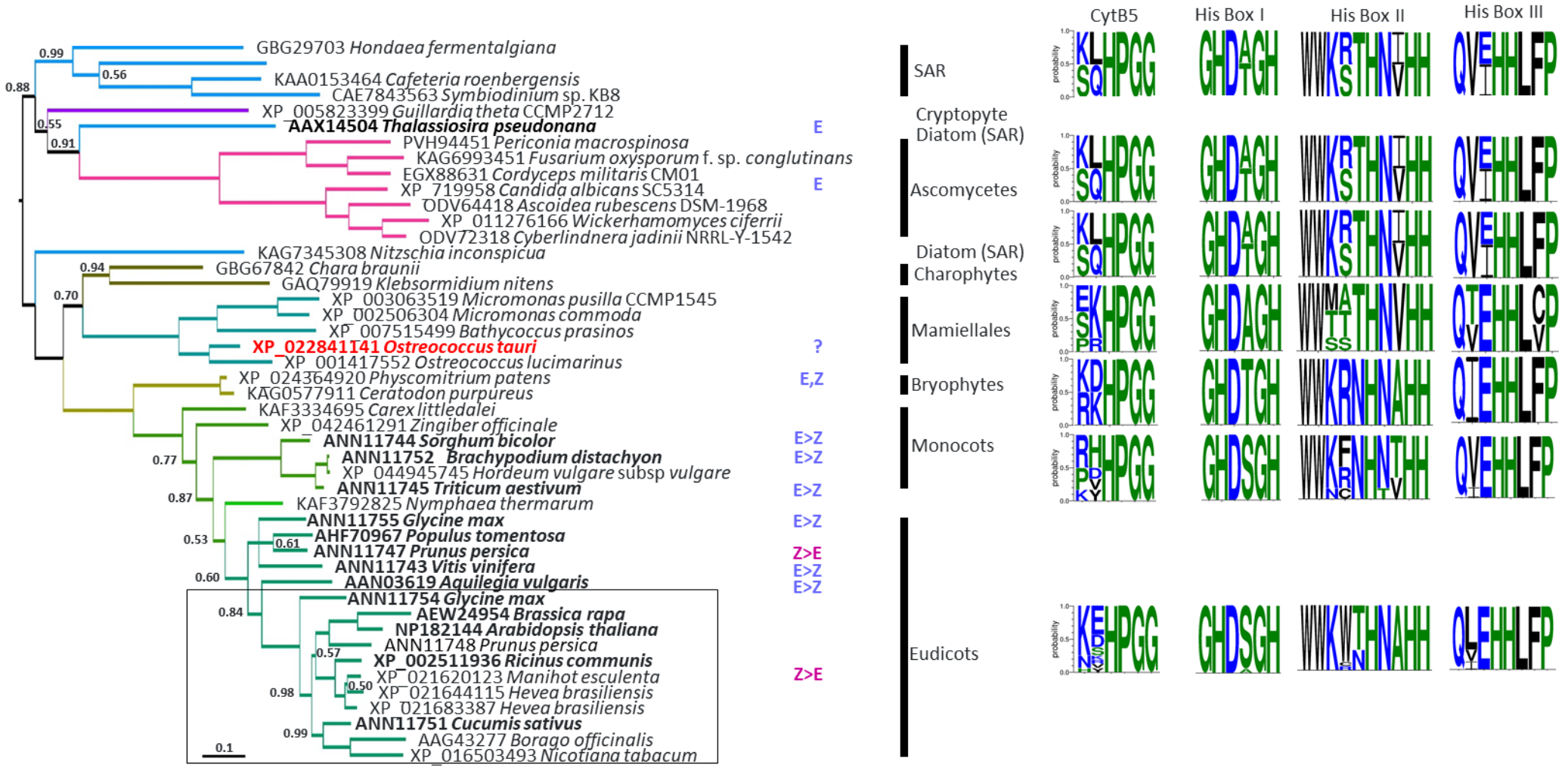

Figure 4. Bayesian phylogenetic tree of sphingolipid Δ8 desaturases.

The tree was drawn to scale in substitutions per site (scale bar on the figure). Posterior Probabilities (2.000.000 generations) lower than 1.00 are indicated by the nodes. Vertical bars indicate taxonomic assignment, also visualised by brench colors. The preference of the enzyme to catalyse the *E*- or *Z*-isomer is indicated on the figure and is based on functional characterisation of the protein (Tonon et al 2005, Oura et al 2008, Li et al 2016). According to Steinberg (2021) the occurrence of *E* and *Z* in *P. patens* is indicated. Sequence logos of the previously identified histidine boxes are presented on the right-hand side. The letter hights are drawn in scale to the probability of occurrence in the sequences used for the sequence logo production (SAR n = 4; Ascomycetes n = 7; Charophytes n = 2; Mamiellales n = 5; Bryophytes n = 2; Monocots n = 7; eudicots n = 16).

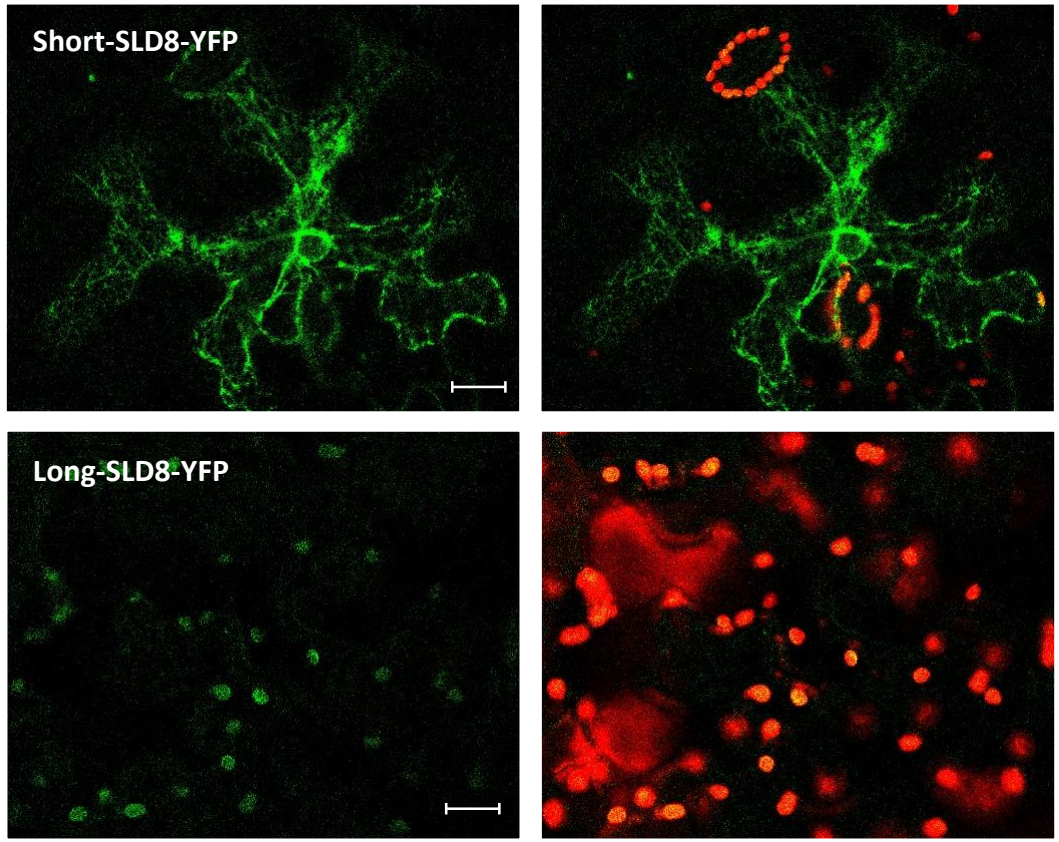

Figure 5. Sub-cellular localisation of *O. tauri* sphingolipid Δ8-desaturase short and long versions in *Nicotiana benthamiana*.

Confocal images of *Nicotiana benthamiana* leaves transiently transformed with OtSLD8-YFP constructs. *O. tauri* sphingolipid Δ8-desaturase short and long versions were cloned into the pK7YWG2 destination vector, the resulting constructs transferred into the *Agrobacterium tumefaciens* strain GV3101, and transformants used for transient expression in leaves. Images were taken 2 days post infiltration. Left, YFP signal; Right, merged of YFP signal and chlorophyll autofluorescence. Bars = 20µm.

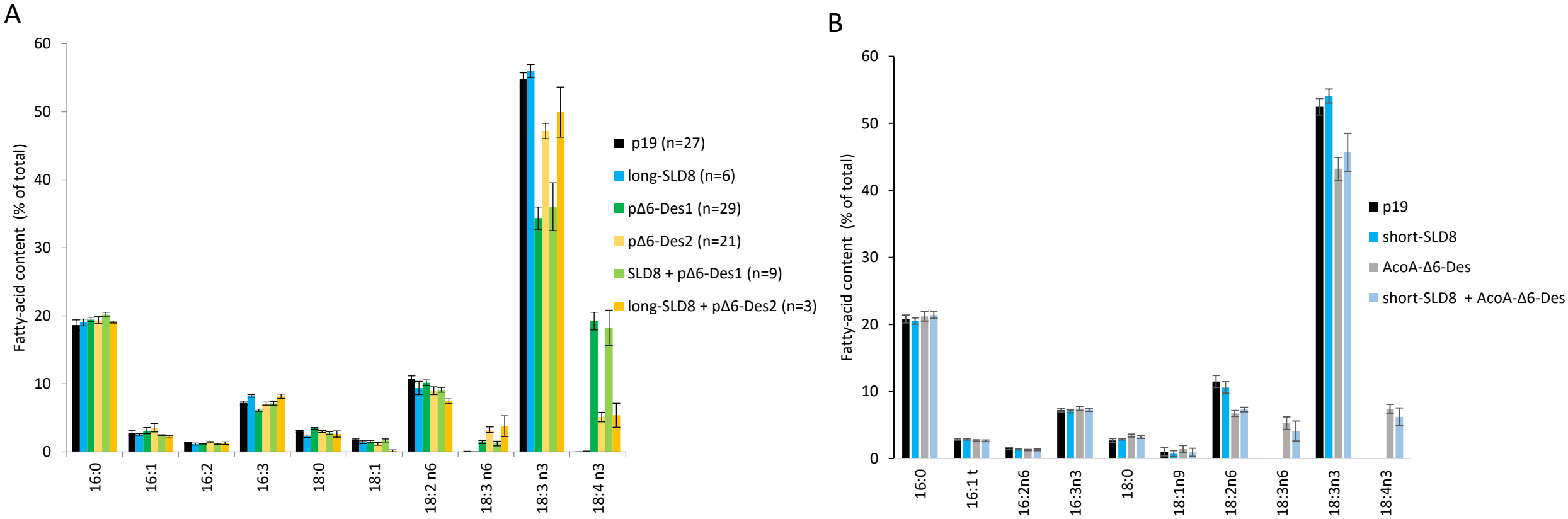

Figure 6. Fatty-acid profile of *N. benthamiana* expressing SDL8 alone and together with Δ6-desaturases.

The anti-silencing protein p19 was used in all infiltrations. **A**. The long-SLD8 (plastid located) was expressed alone and together with the plastidial Δ6 desaturases pΔ6-Des1 and pΔ6-Des2. The number of replicate is indicated. **B**. The short version of SLD8 (ER located) was expressed alone and together with the ER Acyl-CoA-Δ6-Des (ACoA-Δ6-Des) (n=3). Means and standard errors are shown.

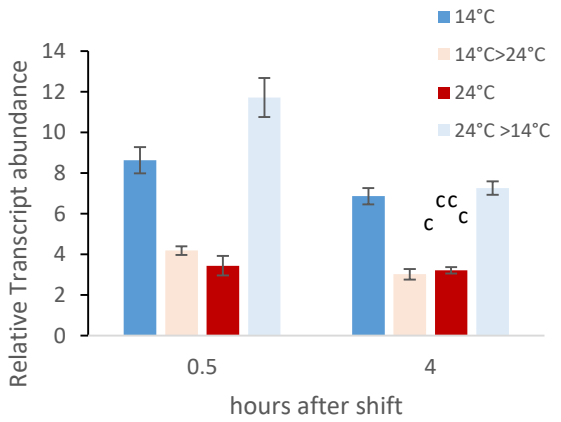

Figure 7. Effect of temperature on SLD8 expression.
Exponentially growing cells were shifted from 24°C to 14°C and reversed while control cells were maintained at the initial temperatures. Cells were harvested 0.5 and 4 h after the temperature shift. Means and standard deviations of technical triplicate are shown. Experiment was repeated twice.

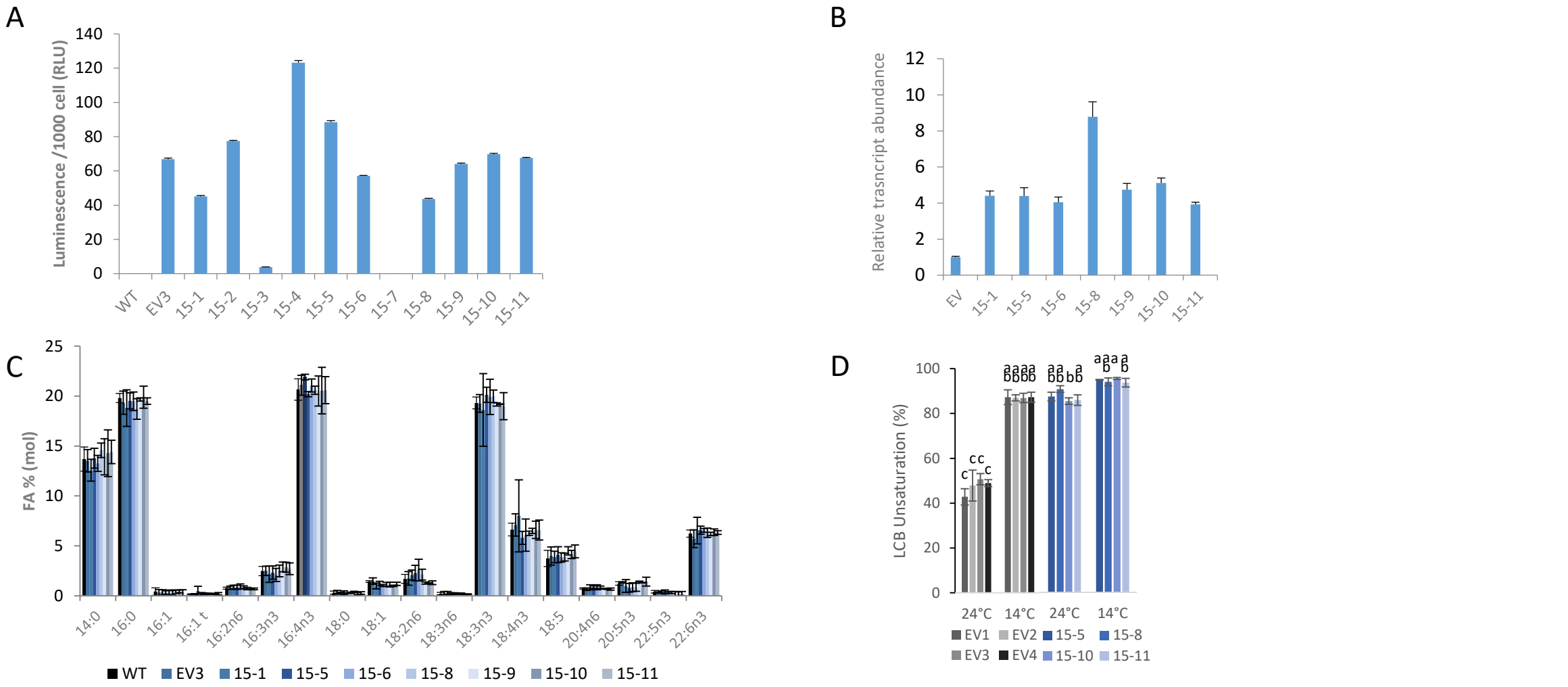

Figure 8. Selection and lipidic analysis of SLD8 overexpressors.

Transgenics are labelled 15-n for SLD8 and EV for the empty vector. **A.** Luminescence of SLD8 transgenics. The Potos-Luc vector carries the luciferase under the CCA1 promoter allowing the selection of lines according to their luminescent level. The line EV3 containing the empty vector (v3 in Fig. S4C) was chosen as negative control for lipid analysis because it produces as much luminescence as SLD8-OEs (Fig. S4C). Means and standard deviation of technical triplicate are shown. **B.** SLD8 relative transcript levels in selected luminescent lines. **C.** Fatty-acid profiles of SLD8 overexpressing lines. **D.** LCB unsaturation rate in control lines (grey) and SLD8 overexpressing lines (blue). Means and standard deviations of culture triplicate are shown. Values were compared among the different transgenics according to Tukey test at $p < 0.05$ and groups with the same letter are not detectably different.

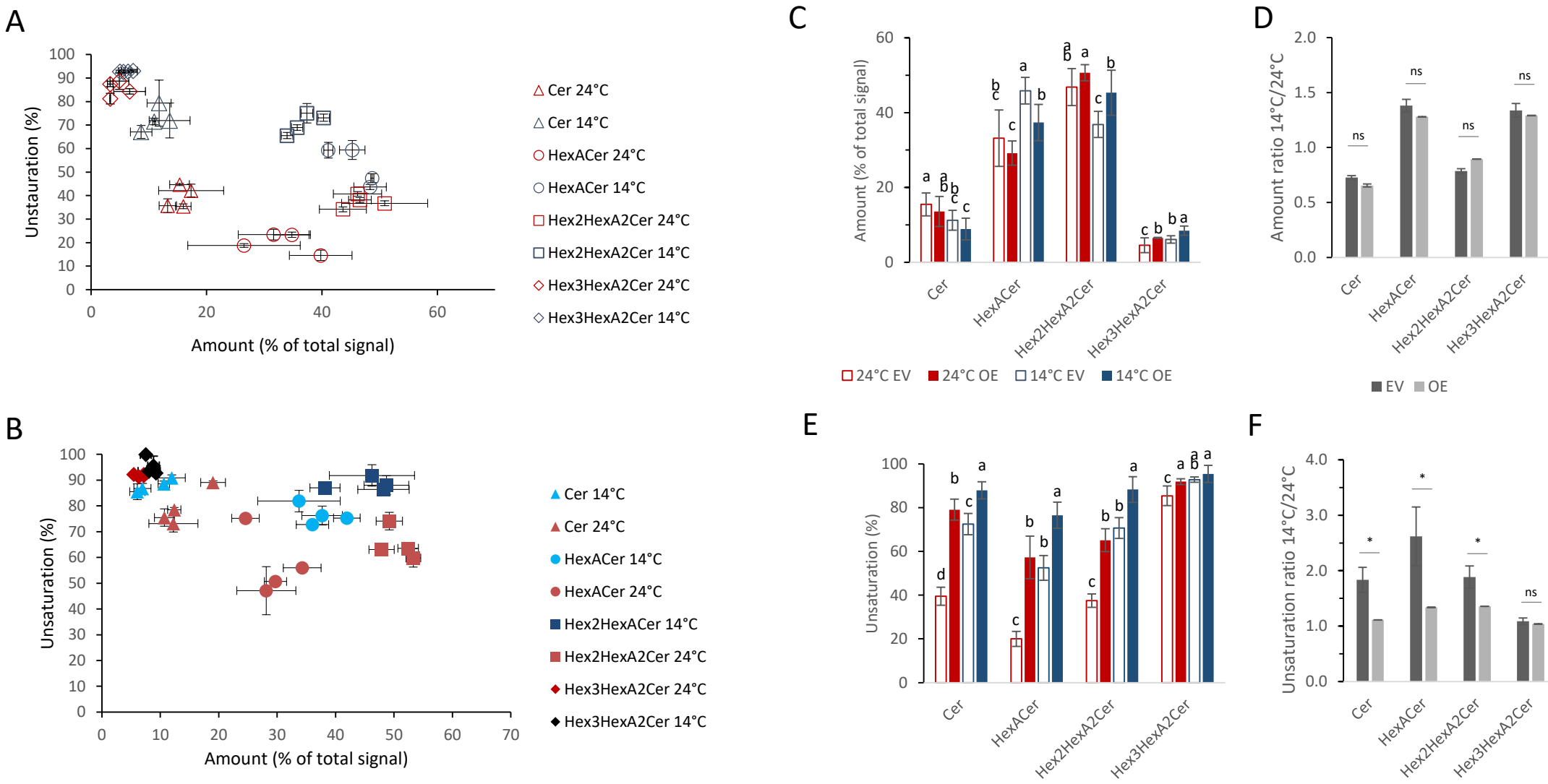

Figure 9. Sphingolipid contents and unsaturation rates in control and SLD8 overexpressing lines as a function of temperature.

Four individual lines where cultivated in triplicate for each, negative controls (EV1,EV2,EV3,EV4, open colored symbols) and SLD8-OEs (15-5, 15-8, 15-10, 15-11 plain colored symbols). Cells acclimated at 24°C or at 14°C were collected at the end of exponential growth for analysis. **A-B**. Correlation between sphingolipid unsaturation rate and relative content in individual transgenic lines, control lines (EVs, A), SLD8-OEs (B). Means and standard deviations of independent triplicate are shown. Unsaturation rate is d18:1/(d18:0+d18:1) ×100 (%). **C**. Relative amount of sphingolipids in EVs and SLD8-OEs at 14°C and 24°C. **D**. Ratio of relative amount between 14°C and 24°C. **E**. Unsaturation rate in sphingolipid classes in EVs and SLD8-OEs at 14°C and 24°C. Errors bars for ratio z=x/y in D and F were calculated according to the error propagation rule $\Delta z = z\sqrt{(\Delta x/x)2+(\Delta y/y)2}$. From C to F, averages of the values from the 4 triplicates of EV lines (n=12) and SLD8-OE lines (n=12) are shown, errors bars are SD. Stastistical significances were calculated within each SL class using the Tukey test in C and E ($p < 0.05$), groups with the same letter are not detectably different, and using the pair-wise Student's t-test) in D and F ($p < 0.05$, ns is not significant).

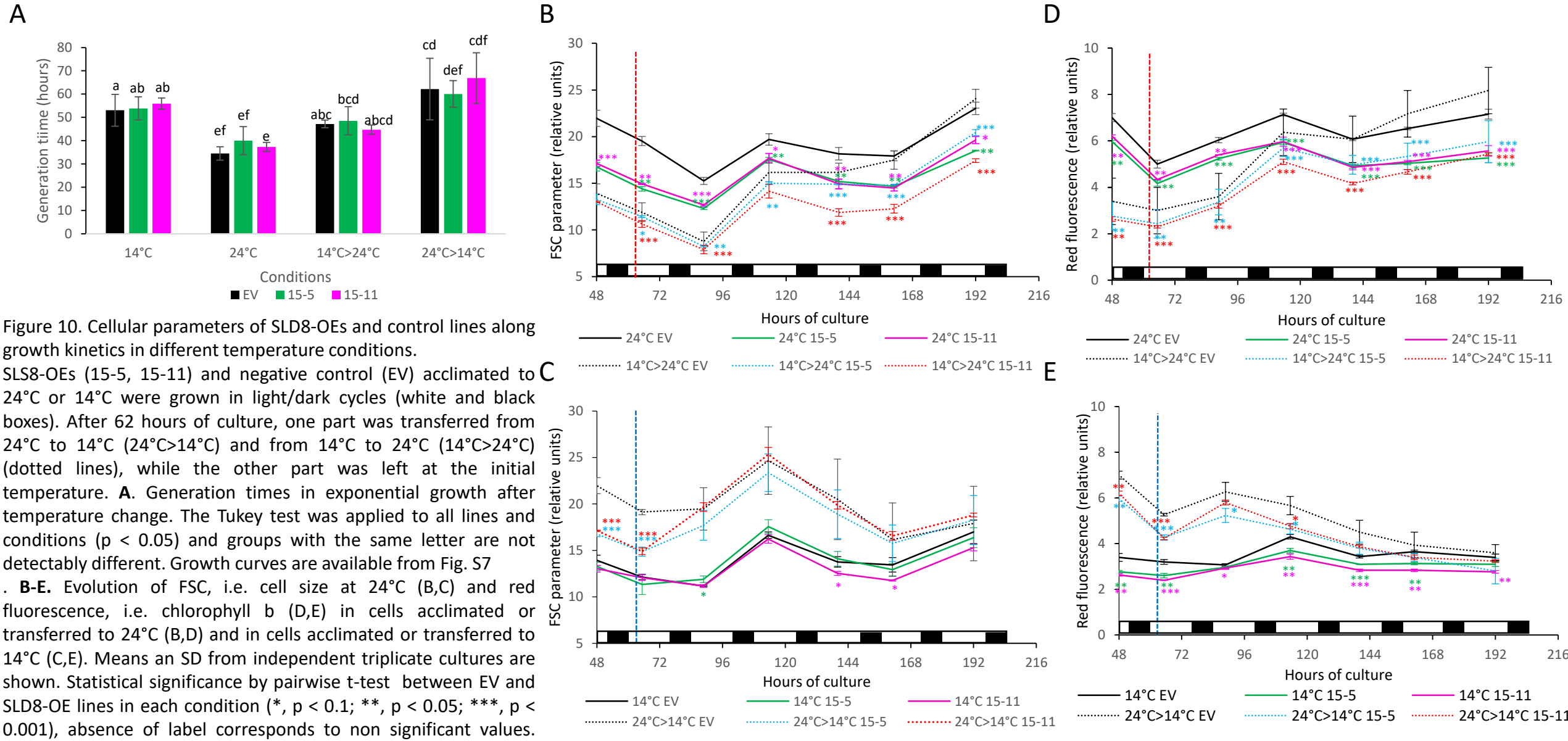

Figure 10. Cellular parameters of SLD8-OEs and control lines along growth kinetics in different temperature conditions.

SLS8-OEs (15-5, 15-11) and negative control (EV) acclimated to 24°C or 14°C were grown in light/dark cycles (white and black boxes). After 62 hours of culture, one part was transferred from 24°C to 14°C (24°C>14°C) and from 14°C to 24°C (14°C>24°C) (dotted lines), while the other part was left at the initial temperature. **A**. Generation times in exponential growth after temperature change. The Tukey test was applied to all lines and conditions ($p < 0.05$) and groups with the same letter are not detectably different. Growth curves are available from Fig. S7

. **B-E.** Evolution of FSC, i.e. cell size at 24°C (B,C) and red fluorescence, i.e. chlorophyll b (D,E) in cells acclimated or transferred to 24°C (B,D) and in cells acclimated or transferred to 14°C (C,E). Means an SD from independent triplicate cultures are shown. Statistical significance by pairwise t-test between EV and SLD8-OE lines in each condition (*, $p < 0.1$; **, $p < 0.05$; ***, $p < 0.001$), absence of label corresponds to non significant values. Vertical dotted lines represent the time of warming (red) and chilling (blue). Evolution of the SSC parameter and complementary representations are available from Fig S8.

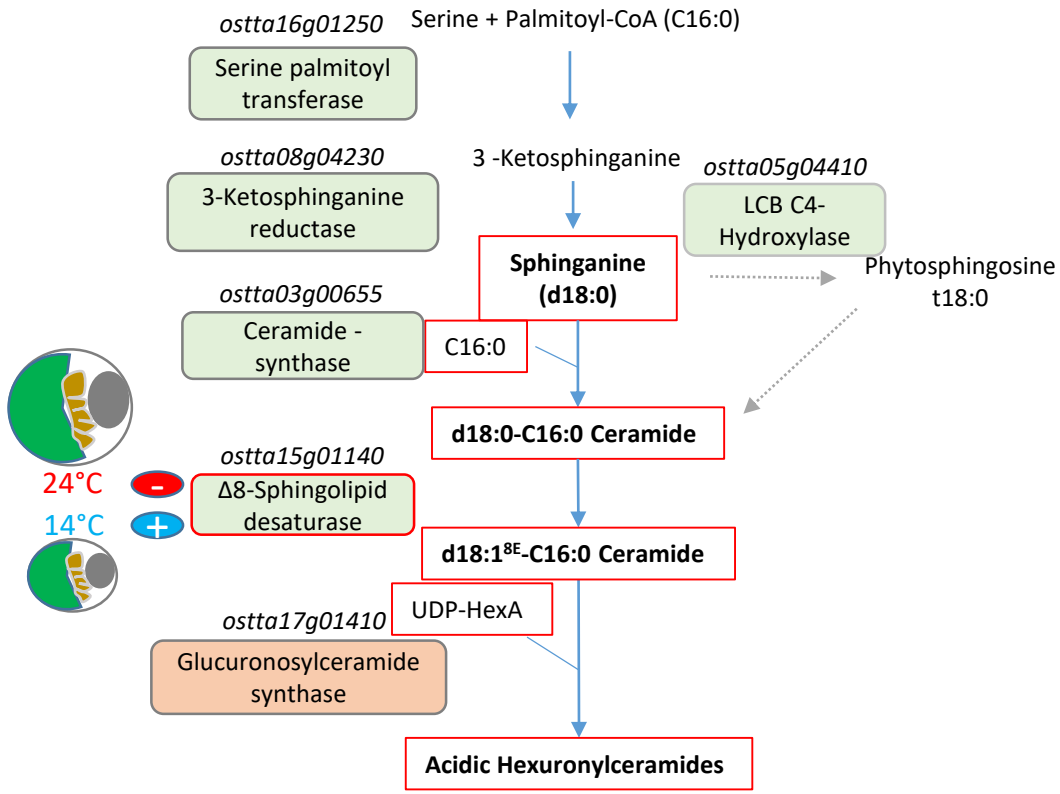

Fig. 11. Sphingolipid pathway in *O. tauri*.
Enzymes involved in the metabolic step are indicated and corresponding genomic accession are indicated (italics). Homologues with E-values ≤ 9.00E-07 and query cover ≥ 41% are indicated in green boxes when obtained by blasting *A. thaliana* protein accessions and in pink box when obtained by blasting protein accessions from other organisms. Red frames highlight sphingolipids and SLD8 characterised in the present work. Activation and/or repression of SLD8 and LCB-D8-unsaturation by temperature and associated cell-size changes are schematised. Grey arrows represent unvalidated step. Details about blast results are provided in Fig. S9.